

SHALLOW-FLOW OVER CURVED BEDS

by

N. S. SIVAKUMARAN

*R. Pathmanaba Iyer
27-B High Street
Plaistow
London E13 0AD
Tel: 020 8471 5636*

SHALLOW-FLOW OVER CURVED BEDS

BY

N.S. SIVAKUMARAN

A Dissertation submitted in partial fulfillment of the requirement
for the Degree of Doctor of Engineering

Examination Committee : Professor Robert B. Banks (Chairman)
Dr. Tawatchai Tingsanchali (Co-chairman)
Professor Roger J. Hosking
Dr. Huynh Ngoc Phien
Professor Anat Arbhabhirama

Nagalingam Subramaniam Sivakumaran

Nationality : Sri Lankan

Previous Degree : B. Eng., University of Ceylon, Peradeniya, Sri Lanka
M. Eng., Asian Institute of Technology, Bangkok, Thailand

Scholarship donor: His Majesty the King of Thailand

Asian Institute of Technology

Bangkok, Thailand

1981

ACKNOWLEDGEMENTS

I wish to express my deep gratitude and sincere appreciation to my adviser *Professor Robert B. Banks*, President of the Asian Institute of Technology, for his inspiring guidance and encouragement during the research period. I am deeply indebted especially to *Dr. Tawatchai Tingsanchali*—who selected this topic for my research—for his critical review of this dissertation, the many valuable suggestions, and his interest and patience which greatly exceeded the expectation from a co-adviser.

I find no words to thank enough *Dr. Roger J. Hosking*, Professor of Applied Mathematics, for his deep interest, encouragement, invaluable assistance in reviewing the whole work from both the mathematical and physical standpoint, and editing the dissertation.

Sincere appreciation is also due to *Dr. Huynh Ngoc Phien* and *Professor Anat Arbhabhirama* for their encouragement. I am grateful to *Dr. André Daubert*, Chief du Service IMA, Direction des Etudes et Recherches, for his kind acceptance to act as the external examiner and to review the dissertation.

The able assistance that I received from the Water Resources Engineering Laboratory technicians is gratefully acknowledged. Thanks are also due to the Water Resources Engineering Division secretaries for their invaluable help in typing the manuscript.

I also wish to express my gratitude to His Majesty the King of Thailand, who through the Asian Institute of Technology, provided a scholarship for the period of my doctoral programme.

I am grateful to my wife, *Inpah*, a source of constant strength and encouragement throughout the period of my programme, and my parents, grandmother and brother for their sacrifices in order to fulfill my educational objectives.

Finally, I thank my friends who helped me to successfully complete the experiments, and I am proud to dedicate this work to them. *Will they read it!*

ABSTRACT

General equations are derived for shallow-flow over a two-dimensionally curved bed; the Saint-Venant and the recent Dressler equations are recovered as special cases. The concept of Froude number is generalized, and the validity of the Dressler equations discussed. The Dressler equations are solved for steady flow, including transition profiles. Application of these equations to a tested spillway crest reproduces its head-discharge relationship and the pressure distribution in remarkable agreement with the experimental data. Predictions for a spillway toe also compare with earlier theory and experiment. Finally, new experiments were carried out for steady flow over a symmetric and an unsymmetric profile, and the Dressler equations are found to be applicable in the range $-2 \leq kh \leq 0.54$ for steady frictionless flow over curved beds. Roll waves in curved bed open channels are briefly discussed in an appendix.

TABLE OF CONTENTS

Acknowledgements	ii
Abstract	iii
Table of Contents	iv
List of Symbols	v
I INTRODUCTION	1-1
II LITERATURE REVIEW	2-2
III THEORY OF SHALLOW-FLOW OVER CURVED BEDS	
3.1 Basic Assumptions and Fundamental Equations	3-1
3.2 Geometry	3-2
3.3 Shallow-Flow Assumptions	3-6
3.4 General Shallow-Flow Equations	3-6
3.5 Special Cases	
3.5A Saint-Venant Equations	3-8
3.5B Dressler Equations	3-8
3.6 Generalized Froude Number	3-10
3.7 Validity of the Dressler Equations	3-11
IV STEADY SOLUTIONS OF THE DRESSLER EQUATIONS	
4.1 Steady Flow	4-1
4.2 Stability	4-3
4.3 Transition Profile	4-5
4.4 Flow Over a Spillway Crest	4-7
4.5 Flow Over a Spillway Toe	4-9
V EXPERIMENT	
5.1 Experimental Setup	5-1
5.2 Measurements	5-1
(PLATES-I, II & III appear between pages 5-4 and 5-5)	
5.3 Experimental Data and Theory	5-5
5.4 Results and Discussion	
5.4A Symmetric Profile	5-6
5.4B Unsymmetric Profile	5-15
VI CONCLUSIONS AND RECOMMENDATIONS	
6.1 Conclusions	6-1
6.2 Recommendations	6-1
Appendix-A On the Geometry of Curved Bed Profiles	A-1
Appendix-B Roll Waves	B-1
References	R-1

LIST OF SYMBOLS

The page numbers in this list refer to the pages on which the symbols first appear. For those symbols having more than one meaning, an entry is made at each appropriate page number. See, for example, the symbol h listed opposite page numbers 1-1, 2-1 and 2-5.

Subscripts h , 0 (or o) denote values at the free surface and at the bed respectively.

Bold type signifies vector or matrix character.

Page	Symbol	Meaning
1-1	κ	bed curvature
	h	flow depth normal to bed
2-1	x, z	horizontal and vertical coordinate
	t	time
	ζ	bed level from $z = 0$
	g	gravitational acceleration
	h	flow depth measured vertically
	u, w	flow velocity components in x, z -directions
	Ξ	defined by
	q	flow rate per unit channel width
	E	total energy head
	ϕ, ψ -axes	streamline and equipotential line
	h_ϕ, h_ψ	scale factors in ϕ, ψ -directions
	κ_ϕ, κ_ψ	curvatures of equipotential line and streamline
	v	flow speed along streamline
	$\mathbf{\kappa}$	$(-\kappa_\psi, \kappa_\phi)$
2-3	p	pressure
	ρ	fluid density
	a	vertical acceleration of flow
	\mathbf{k}	unit basis in z -direction
	$\mathbf{0}$	null vector in xz -frame
	$f(x)$	function of x

Page	Symbol	Meaning
2-4	n	coordinate normal upwards from bed
	r	radius of curvature of streamline
	R	hydraulic mean radius
	C, n $ $	Chézy and Manning roughness coefficients magnitude (modulus)
2-5	s	arc length measured downstream along curved bed
	h	flow depth normal to bed
	u_0	flow velocity at bed
	θ	bed slope
2-6	u, w	flow velocity components in s, p -directions
	X	Kh
	\tilde{f}	Dressler's local Froude number
	\tilde{f}_s	$P_0 < P_h$ when $\tilde{f} > \tilde{f}_s$
	\tilde{f}_e	Dressler equations are elliptic when $\tilde{f} > \tilde{f}_e$
	\tilde{f}_c	Dressler's local critical Froude number
2-7	λ	measure of channel surface roughness
3-1	\mathbf{V}	flow velocity
	$\mathbf{a} \cdot \mathbf{b}$	scalar product of two vectors
	Ω	gravitational potential
	Π	constant atmospheric pressure
3-2	$\mathbf{a} \times \mathbf{b}$	vector product of two vectors
	\mathbf{F}	body force
	R^2	smooth two-dimensional Riemannian manifold
	ξ^1, ξ^2	generally non-orthogonal Gaussian coordinates on R^2
	e	belongs to
	$a_{\alpha\beta}$	metric tensor of R^2 ; $\alpha, \beta \in \{1, 2\}$
3-3	a	determinant of matrix of $a_{\alpha\beta}$
	ϕ	scalar field
	\mathbf{F}	surface vector in R^2
	F^α, F_α	contravariant and covariant components of \mathbf{F} in ξ^α -direction; $\alpha \in \{1, 2\}$
	$e^{\alpha\beta}$	$e^{12} = -e^{21} = 1$ and zero otherwise
	R^3	three-dimensional Riemannian manifold defined by (ξ^1, ξ^2, n)

Page	Symbol	Meaning
	g_{ij}	metric tensor of R^3 ; $i, j \in \{1, 2, 3\}$
	κ_α	normal curvature of R^2 in ξ^α -direction
	J_α	$1 - \kappa_\alpha n$
	g	determinant of matrix of g_{ij}
3-4	e^{ijk}	1 for a cyclic (even) permutation of ijk -1 for an anticyclic (odd) permutation of ijk 0 for any two equal indices
	\mathbf{V}	space vector in R^3
	v^i, v_i	contravariant and covariant components of \mathbf{V} in R^3 defined by (ξ^1, ξ^2, n)
	$g_{\alpha\beta}, g^{\alpha\beta}$	defined by (3.13) and (3.14)
	$a^{\alpha\beta}$	associated contravariant metric tensor of R^2
	v^α, v_α	contravariant and covariant components of flow velocity \mathbf{V} (space vector) in ξ^α -direction
	w	component of \mathbf{V} in n -direction
	θ	angle n makes with z
3-5	ϵ	small positive number $\ll 1$
3-6	\mathbf{G}	second order symmetric matrix defined by (3.24)
	$\delta_{\alpha\beta}, \delta^{\alpha\beta}$	Kronecker delta ($=1$ for $\alpha=\beta$, $=0$ for $\alpha \neq \beta$)
	x, y	coordinates on flat bed, along flow and normal to it
	J	$1 - Kn$
3-9	S	storage (c.f. figure 3.6)
3-10	R	radius of curvature of bed
3-11	c	celerity
	\mathbf{F}	generalized Froude number
	e	base of natural logarithms
	χ_ℓ, χ_u	lower and upper bounds of χ for applicability of Dressler equations
4-1	α	$2g(E-\zeta)/(q\kappa)^2$
	β	$-2g\cos\theta/(q^2\kappa^3)$
	$\gamma(\chi)$	$[(1-\chi)\ln(1-\chi)]^{-2}$
4-2	$\gamma'(\chi)$	$d\gamma/d\chi$
	x or x	horizontal coordinate

Page	Symbol	Meaning
4-3	C_d	discharge coefficient
	S_e	energy slope
4-4	λ	free parameter
	Φ, Ψ	defined by (4.16)
	σ	$q^2 \kappa^3 / g$
	θ_0, χ_0	singular point i.e. solution of $\Phi = \Psi = 0$
	m	defined by (4.17)
4-5	q_n	quasi-normal discharge c.f. (4.21)
	q_c	critical discharge c.f. (4.22)
	h_0, h_c	normal and critical depths in flat bed channel flow
	$T(\chi), m(x), \epsilon(x, \chi)$	defined by (4.25a,b,c)
4-6	$\zeta', \zeta'', \zeta'''$	$d\zeta/dx, d^2\zeta/dx^2, d^3\zeta/dx^3$
4-7	H_d	design head of spillway
	F	$q^2 / (2gH^3)$
	x_n	upper nappe coordinate
	H	operating head of spillway
4-11	h_1, h_2	initial and central depths c.f. figure 4.9
	u_1	initial velocity
	α	$(\kappa h_1)^{-1}$
	Ω	$1 - \kappa h_2$
	P_0	bed pressure at point of symmetry
	C_p	pressure coefficient
	2ϕ	toe angle
	F_1	$u_1^2 / (gh_1)$
	λ	$2a^3 / F_1$
	μ	$a^2 - 2a^2(\alpha - 1)F_1^{-1} \cos\phi$
	P_s	hydrostatic pressure at point of symmetry
4-12	P_c	centrifugal pressure at point of symmetry
	C_s, C_c	hydrostatic and centrifugal pressure coefficients
	$\hat{\Omega}$	root of (4.36)

Page	Symbol	Meaning
5-1	Q	total discharge (cm^3/s)
	H	average level difference in mercury manometer attached to orifice (cm)
5-4	D	water depth at flat bed section (cm)
5-5	x_1	point on x-axis
	ζ_1	$\zeta(x_1)$
	D_1	vertically measured water depth at x_1 (cm)
	$(x_1, z_1 \equiv \zeta_1 + D_1)$	experimental location of free surface
	(x_1, z_1)	theoretical location of free surface on same bed-normal through (x_1, z_1)
	(x_2, ζ_2)	base of bed-normal through (x_1, z_1)
	θ_2, κ_2	bed slope and curvature at (x_2, ζ_2)
	H_2, h_2	experimental and theoretical water depths normal to bed at (x_2, ζ_2)
5-6	α_2, β_2	α, β at (x_2, ζ_2)
	θ_1, κ_1	bed slope and curvature at (x_1, ζ_1)
	α_1, β_1	α, β at (x_1, ζ_1)
	P_0	bed pressure
5-7	P_c	centrifugal pressure
	$\Lambda(\chi)$	defined by (5.15)
	$\Lambda'(\chi)$	$d\Lambda/d\chi$
	$\Delta P_c, \Delta \kappa$	error in centrifugal pressure and in curvature
6-1	f	friction factor
	R	Reynolds number
	ϵ	relative roughness of channel surface
A-1	L	length of model bed profile
	I_i	x -interval $x_i < x \leq x_{i+1}$
	$V_i \equiv (x_i, y_i)$	vertices
	i	$0, 1, \dots, m-1$
	V_0	$(0, 0)$
	V_m	$(L, 0)$
	s	parameter $e \in \{0, 1\}$
	(ξ, ζ)	point on spline curve
	$\xi', \xi'', \zeta', \zeta''$	a prime denotes d/ds

Page	Symbol	Meaning
B-1	x	coordinate downstream along flat bed
	y	coordinate normal upwards from x
	A	flow area
	H	flow depth normal to bed
	u	local flow velocity in x-direction
	U	average of u over H
	θ	channel inclination
	β	momentum coefficient $\equiv (U^2 A)^{-1} \int_A u^2 dA$
	R	hydraulic mean radius
	T	shear stress magnitude at channel surface
Partial derivatives with respect to x, t are denoted by subscripts.		
	dA/dH	free surface width
	A/(dA/dH)	hydraulic depth
B-2	F, f	Froude number and friction factor defined by (B.4)
	a, b, c	constants depend on assumed velocity profile
	k_s	characteristic bed roughness height
	ν	kinematic viscosity of fluid
	R	Reynolds number $\equiv 4UH/\nu$
	F_c	critical Froude number below which no roll waves are formed
	B-3	λ
θ		bed slope
Ω		1-Kh
s		arc length measured downstream along curved bed
F		frictional dissipation
Bar designates steady value		
Partial derivatives with respect to s, t are denoted by subscripts		
B-4	ϕ, η	small perturbations in \bar{q}, \bar{h}
	F	Froude number defined by (3.35)
	L, M, N	defined by (B.16)
	$\alpha, \alpha_r, \alpha_i$	real constants
	i	$\sqrt{-1}$
	$\sigma \equiv \sigma_r + i\sigma_i$	complex phase-velocity
	$\sigma_{r,c}$	critical phase-velocity
	λ	measure of channel roughness

I INTRODUCTION

Open channel hydraulics is one of the oldest disciplines of human civilization. However, it was during the relatively recent Western scientific revolution that the *Saint-Venant* (1871) equations were established to study various problems in open channel flow—uniform, nonuniform, steady or unsteady. The basic assumption is that vertical acceleration of fluid particles is negligible, or equivalently that the vertical pressure distribution is hydrostatic. Although the basic equations are inviscid, energy loss due to friction at channel boundaries has been incorporated by invoking either the *Chézy* (1769) or the *Manning* (1889) formula. The simplicity of the Saint-Venant equations, and their successful application to various problems in hydraulics, has led to their wide acceptance by engineers who by experience tolerate the errors introduced by the basic assumptions.

Using an asymptotic approximation in terms of a "shallowness" parameter, *Friedrichs* (1948) re-derived in a Cartesian frame the Saint-Venant equations for flow over flat beds. *Keller* (1948) applied Friedrichs' method to two- and three-dimensional flows over curved bed channels, and obtained higher-approximation equations that are either not very different from Saint-Venant or otherwise difficult to solve. On the other hand potential theory conformal mapping techniques applied to flow over curved beds, such as spillways and sills, theoretically demonstrated the importance of bed curvature. However these solution procedures are usually lengthy, and there is no convenient way of including viscous dissipation.

Recently *Dressler* (1978) produced new shallow-flow equations with bed curvature by applying an asymptotic approximation in terms of a "shallowness" parameter to the exact formulation of the problem in curvilinear coordinates—one coordinate directed along the bed and the other normal upwards from it. In terms of a local Froude number, he identified regions of flow separation, subcritical flow, and supercritical flow. He suggested the range $-0.85 \leq Kh \leq 0.5$ (K : bed curvature, h : free surface location normal to the bed) for applicability of his equations, subject to future experimental verification.

After a detailed literature review in *Chapter II*, this thesis emphasises theoretical and experimental work on the Dressler equations. In *Chapter III* the generalized shallow-flow equations are derived for flow over a two-dimensional Riemannian manifold; the Saint-Venant and Dressler equations are recovered as special cases. Further, the concept of Froude number is generalized, and the validity of the Dressler equations discussed. In *Chapter IV*, steady solutions of the Dressler equations are obtained, and applied to steady flow over an experimentally tested spillway crest and spillway toe. New experiments to verify the Dressler equations, involving steady flow over a symmetric and an unsymmetric bed profile, are described in *Chapter V*. Conclusions and recommendations are presented in *Chapter VI*. The experimental bed geometry of *Chapter V* is detailed in *Appendix A*, and roll waves over curved bed open channels are briefly discussed in *Appendix B*.

II LITERATURE REVIEW

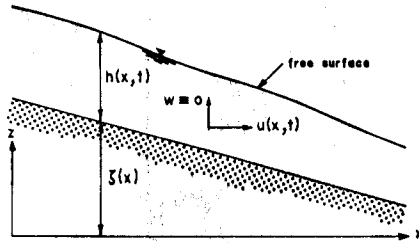


Figure 2.1 Definition sketch: Saint-Venant equations

For more than a century, almost all open channel flow analyses have been based upon the Saint-Venant (1871) equations (for a rectangular channel; figure 2.1) viz.

$$\text{continuity, } \frac{\partial h}{\partial t} + \frac{\partial q}{\partial x} = 0, \quad q \equiv uh = \text{flow per unit width.} \quad (2.1)$$

$$\text{momentum, } \frac{\partial u}{\partial t} + g \frac{\partial E}{\partial x} = 0, \quad E \equiv \zeta + h + \frac{u^2}{2g} = \text{total energy head.} \quad (2.2)$$

The classical derivation of these equations (Lamb (1945), Stoker (1948) and Fox (1977)) assumes *two-dimensional incompressible irrotational inviscid flow in the constant gravitational field*, over a *linear bed* (either horizontal or with only a small inclination, $\partial \zeta / \partial x$), with *negligible particle acceleration in the vertical direction of flow*.

In fact, the vertical acceleration is negligible (i.e. the vertical pressure distribution is hydrostatic and the vertical velocity component vanishes identically) whenever the streamlines have neither substantial curvature nor divergence. From figure 2.2, the respective intrinsic equations of continuity and irrotationality are

$$\frac{\partial}{\partial \phi} (h_\psi v) = 0 \quad \text{or} \quad \frac{1}{h_\phi} \frac{\partial v}{\partial \phi} + \kappa_\psi v = 0,$$

$$\frac{\partial}{\partial \psi} (h_\phi v) = 0 \quad \text{or} \quad \frac{1}{h_\psi} \frac{\partial v}{\partial \psi} - \kappa_\phi v = 0,$$

where $\kappa_\psi = \frac{1}{h_\psi h_\phi} \frac{\partial h_\psi}{\partial \phi}$ and $\kappa_\phi = -\frac{1}{h_\phi h_\psi} \frac{\partial h_\phi}{\partial \psi}$ are respectively the curvatures of the equipotential line and the streamline (figure 2.3); equivalently

$$\text{grad } v = v \mathbf{K}, \quad \mathbf{K} = (-\kappa_\psi, \kappa_\phi).$$

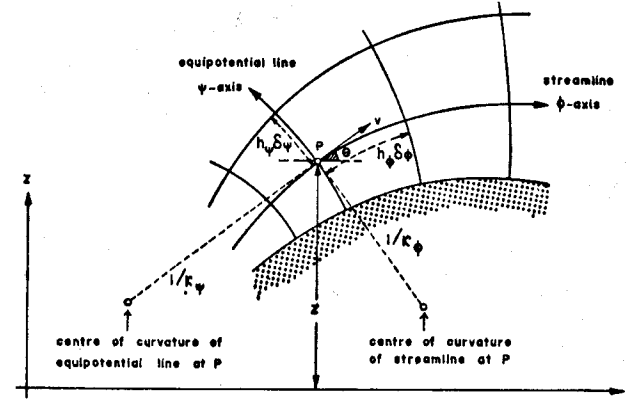
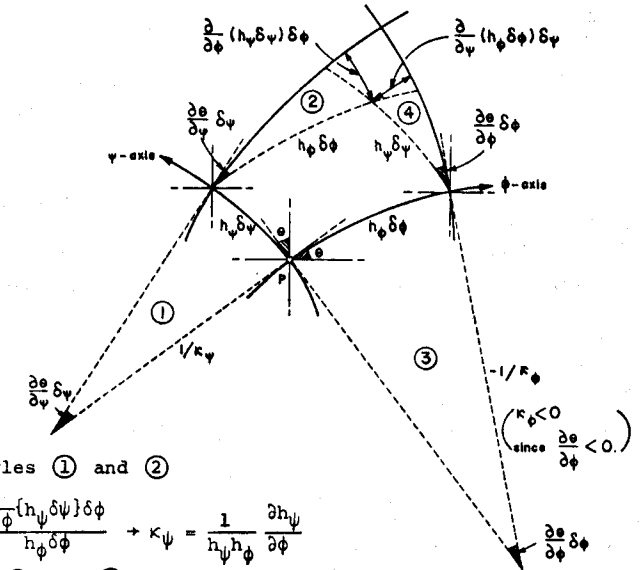


Figure 2.2 Definition sketch: intrinsic equations.



From similar triangles ① and ②

$$\frac{h_\psi \delta \psi}{1/\kappa_\psi} = \frac{\frac{\partial}{\partial \phi} (h_\psi \delta \psi) \delta \phi}{h_\phi \delta \phi} \rightarrow \kappa_\psi = \frac{1}{h_\psi h_\phi} \frac{\partial h_\psi}{\partial \phi}$$

and similarly from ③ and ④

$$\frac{h_\phi \delta \phi}{-1/\kappa_\phi} = \frac{\frac{\partial}{\partial \psi} (h_\phi \delta \phi) \delta \psi}{h_\psi \delta \psi} \rightarrow \kappa_\phi = -\frac{1}{h_\phi h_\psi} \frac{\partial h_\phi}{\partial \psi}.$$

Figure 2.3 κ_ψ and κ_ϕ

Hence from Euler's equation of steady motion under gravity

$$-\text{grad}(p+\rho gz) = \rho v \text{ grad } v = \rho v^2 \kappa,$$

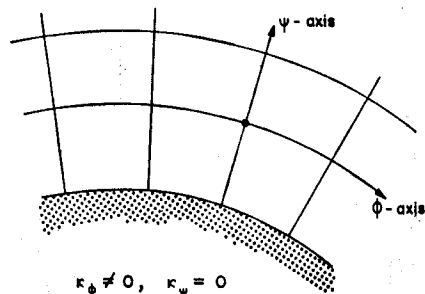
the vertical acceleration a_z is

$$-\frac{\partial}{\partial z}(p+\rho gz) = a_z = \rho v^2 \kappa \cdot \mathbf{k} \quad (\mathbf{k}: \text{vertical unit basis})$$

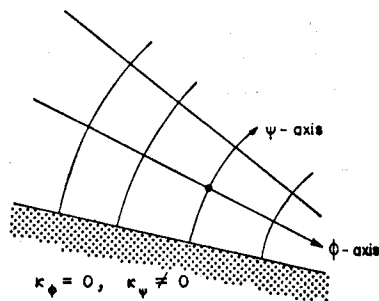
$$\text{or } a_z = 0 \leftrightarrow \kappa = 0 \leftrightarrow p+\rho gz = f(x). \quad (2.3)$$

Therefore strictly speaking (2.2) is applicable with great accuracy to gradually varied flow (since the change in depth of flow is so mild that the streamlines have neither appreciable curvature ($\kappa_\phi \approx 0$) nor divergence ($\kappa_\psi \approx 0$)) as well as to uniform flow.

Further, the kinematic boundary conditions at both the curved bed and the non-horizontal free surface are violated, since (2.3) defines the instantaneous streamlines to be straight and horizontal.



Case of substantial streamline curvature



Case of streamline divergence

Friedrichs (1948) re-derived the Saint-Venant equations for flow over a flat horizontal bed, using asymptotic approximations in terms of a "shallowness" parameter, and Keller (1948) obtained equations for two- and three-dimensional flows over a curved bed. However, Keller's equations for two-dimensional flow are similar to (2.1) and (2.2), with the slight nonlinear bed effects only accounted for by the term $\partial \zeta / \partial x$. Keller did derive higher-order approximate equations by extending this asymptotic method to better include the effects of bed curvature, but these equations proved difficult to solve and have not been exploited by engineers, (Dressler, 1978).

Another approach is to treat flow over a curved bed by potential theory. Watters and Street (1964) considered two-dimensional steady ideal fluid flow over sills in open channels. By means of complex functions and conformal mapping, they developed a theory for flow over a single step, then extended it to flow over a sill made out of finite line segments, and finally generalized it to flow over a smooth sill. Their general theory enables the calculation of velocity, pressure and free surface location for an arbitrary local change in the channel bed.

Cassidy (1965) studied irrotational flow over circular weirs, and spillways of finite height shaped after weir-nappe profiles; he suggested a numerical technique to solve the Laplace equation. His work involved the mapping of the problem into the complex-potential plane (rectangular), the sketching of an initial approximate flow net, and the use of numerical methods. Although his theoretical discharge coefficients for irrotational flow were slightly but notably greater than experimentally measured values, the pressure and velocity distributions and free surface coordinates were in remarkable agreement with experiment. Curves for minimum pressure on the spillway surface were also developed in this study. However, the required computer storage and time (≈ 6 hours) were high.

Ali (1972) investigated flow over rounded spillways, assuming the velocity distribution $\partial v / \partial n = v/r$ (consistent with irrotational flow); linear variation of streamline curvature (r) between the upper and lower nappes, parabolic or cubic forms of normals to the streamlines; and cubic form for the upper nappe (free surface). This approach does not require any initial approximate flow net. He found that the choice of parabolic normal (in this event the discharge need not be known) greatly simplified the solution, and that the experimental upper nappe can be fitted quite well by general cubic equations. His calculated discharges, pressure and velocities agreed well with experimental results provided that these were measured downstream of the crest. The required computer time was around one minute.

Flow in open channels with smooth curved boundaries was analysed by Moayeri (1973). He derived a pair of integro-differential equations expressing the potential flow over a smooth step in open channels in terms of the approach Froude number, and an unknown distribution of elevation as a function of velocity potential on the flow boundaries. Numerical solutions using appropriate quadrature and differentiation formulae were obtained for flows with approach Froude number $F = 0.4$ and 1.7 . Free surface geometry, flow net and pressure distribution were also given for each value of F .

As pointed out by many investigators, (including Watters and Street (1964), and Ali (1972)), the flow of a real liquid with air above its free surface has several complications. For example, in the case of spillways, the development of a turbulent boundary layer downstream of the crest, and the consequent aeration of the flow, are governed by viscosity of the liquid and the roughness of the solid boundary, amongst other parameters. Unfortunately, there is no convenient way of modifying potential theory to include the non-conservative viscous dissipation. On the other hand, friction may be treated as an external force in the Euler's equation; an extra term (as given appropriately by the Chézy or Manning formula) representing lumped frictional effects may be "glued" to Saint-Venant and Keller equations. For example, the Saint-Venant equation (2.2) becomes

$$\frac{1}{g} \frac{\partial u}{\partial t} + \frac{\partial E}{\partial x} = \begin{cases} -\frac{u|u|}{C^2 R} & : \text{Chézy (1769) friction term,} \end{cases} \quad (2.4)$$

$$\begin{cases} -\frac{u|u|}{n^2 R^{4/3}} & : \text{Manning (1889) friction term,} \end{cases} \quad (2.5)$$

where C and n are Chézy and Manning roughness coefficients, respectively; and R is the hydraulic mean radius. However, the lack of attention to bed curvature effects may make these classical equations inaccurate.

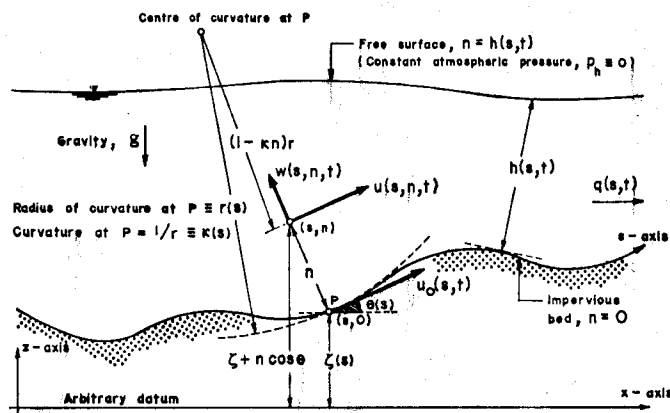


Figure 2.4 Definition sketch: Dressler's derivation

Dressler (1978) derived new nonlinear shallow-flow equations with bed curvature; used (s, n) coordinates, where s is the arc length measured downstream along the curved bed, and n is normal upwards from it; figure 2.4. He relaxed the assumptions of linear bed and negligible vertical acceleration of particles; and applied the more familiar types of boundary layer asymptotics (Prandtl (1905), Friedrichs and Dressler (1961)) to the exact formulation of the flow problem, by introducing new independent variables (see p.3-6) that stretch the flow domain to keep it from vanishing as the shallowness parameter approaches its limit.

Dressler's first order results are (figure 2.4):

$$\frac{\partial h}{\partial t} + \frac{1}{(1-Kh)^2} u_0 \frac{\partial h}{\partial s} - \left(\frac{\ln(1-Kh)}{(1-Kh)K} \right) \frac{\partial u_0}{\partial s} + \frac{1}{K^2} \frac{dK}{ds} \left(\frac{Kh}{(1-Kh)^2} + \frac{\ln(1-Kh)}{1-Kh} \right) u_0 = 0, \quad (2.6)$$

$$\frac{\partial u_0}{\partial t} + \frac{1}{(1-Kh)^2} u_0 \frac{\partial u_0}{\partial s} + \left(g \cos \theta + \frac{Ku_0^2}{(1-Kh)^3} \right) \frac{\partial h}{\partial s} - \left(Kg \sin \theta - \frac{dK}{ds} \frac{u_0^2}{(1-Kh)^3} \right) h + g \sin \theta = 0, \quad (2.7)$$

where

$$u(s, n, t) = \frac{u_0(s, t)}{1-Kn} \quad (2.8)$$

$$w(s, n, t) = \left(\frac{\ln(1-Kn)}{(1-Kn)K} \right) \frac{\partial u_0}{\partial s} - \frac{1}{K^2} \frac{dK}{ds} \left(\frac{Kn}{(1-Kn)^2} + \frac{\ln(1-Kn)}{1-Kn} \right) u_0 \quad (2.9)$$

and

$$p(s, n, t) = \rho g (h-n) \cos \theta + \frac{1}{2} \rho u_0^2 \left(\frac{1}{(1-Kh)^2} - \frac{1}{(1-Kn)^2} \right) \quad (2.10)$$

Also, he derived the mass conservation relation

$$(1-Kh) \frac{\partial h}{\partial t} + \frac{\partial q}{\partial s} = 0, \quad q \equiv \int_0^h u \, dn = -\frac{u_0}{K} \ln(1-Kh), \quad (2.11)$$

from (2.6) and (2.8); we have shown (see Section 3.5B) that this could be realized independently from the principle of mass conservation itself. Moreover, his momentum equation (2.7) failed to exhibit compactness in terms of any physically understandable quantity.

Dressler showed that his equations are hyperbolic¹, and give the Saint-Venant equations as the bed curvature approaches zero. With the definition of a local Froude number ($f = u_0^2 / gh \cos \theta$; figure 2.5) he identified regions of flow separation; and supercritical and subcritical flows.

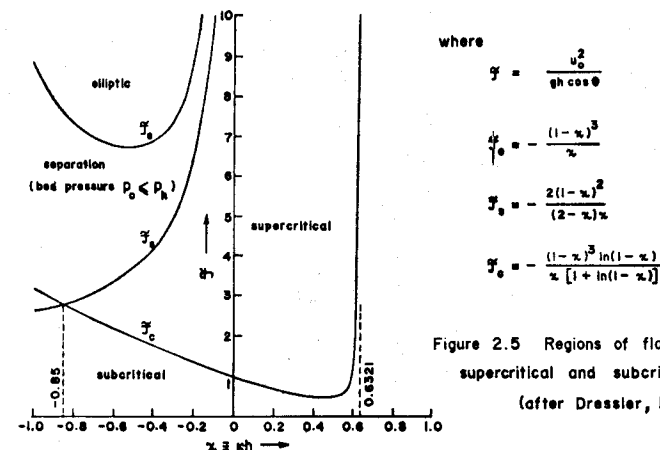


Figure 2.5 Regions of flow separation; and supercritical and subcritical flow (after Dressler, 1978)

¹ The type of a partial differential equation is an invariant under frame transformations.

Further, by assuming the drag at the channel surface as $-\lambda u^2(s,n,t)$, he suggested a generalization of the Chézy formula for *wide channels*; and mentioned that the term

$$-\frac{\lambda u_o^2}{gh} \left(1 - \frac{kh}{2}\right) \quad (2.12)$$

where $\begin{cases} \lambda : \text{measure of roughness,} \\ h : \text{"hydraulic radius" (wide channels),} \end{cases}$

can be added to the right hand side of his momentum equation (2.7) when needed. He also stated that, for steady flow, the new equations define a generalization of the Bresse (1860) profile equation, when a Chézy resistance term (modified for curvature) is added.

Dressler did not present any experimental verification of his theory, but tentatively suggested the range

$$-0.85 \leq kh \leq 0.5 \quad (2.13)$$

subject to experimental check.

III THEORY OF SHALLOW-FLOW OVER CURVED BEDS

The fundamental flow equations in vector form stated below are first represented in general coordinates suitable for flow over a curved bed (a two-dimensional Riemannian manifold). General shallow-flow equations are then derived, and the Saint-Venant and the Dressler equations are recovered as special cases. The theoretical validity of the Dressler equations is discussed in terms of a generalized Froude number.

3.1 Basic Assumptions and Fundamental Equations

For an incompressible irrotational inviscid flow under constant gravity (g) with a stable free surface of negligible surface tension, over an impervious stationary bed, the fundamental governing equations are:

$$\text{div } \mathbf{v} = 0 \quad (\text{continuity}) \quad (3.1)$$

$$\frac{\partial \mathbf{v}}{\partial t} + \text{grad}(gE) = 0 \quad (\text{momentum}) \quad (3.2)$$

$$\text{curl } \mathbf{v} = 0 \quad (\text{irrotationality}) \quad (3.3)$$

subject to boundary conditions of kinematic type:

$$\frac{\partial h}{\partial t} + \mathbf{v}_h \cdot \text{grad } h = w_h \quad (\text{stable free surface}) \quad (3.4)$$

$$w_0 = 0 \quad (\text{impervious stationary bed}), \quad (3.5)$$

and of dynamic type:

$$p_h = \Pi \quad (\text{negligible surface tension}), \quad (3.6)$$

where the subscripts $h, 0$ denote values at the free surface and at the bed respectively (this notation is used throughout this chapter) and

$$\begin{aligned} t &- \text{time} \\ \mathbf{v} &- \text{flow velocity} \\ E &- \text{total energy head, } gE \equiv \Omega + \frac{p}{\rho} + \frac{\mathbf{v}^2}{2} \\ \Omega &- \text{gravitational potential} \\ p &- \text{pressure} \\ \rho &- \text{fluid density} \\ n &- \text{normal coordinate from the bed (c.f. figure 3.1)} \\ h &- \text{flow depth normal to the bed} \\ w &- \text{velocity component in the } n\text{-direction} \\ \Pi &- \text{constant atmospheric pressure} \end{aligned} \quad (3.7)$$

In deriving (3.2), we make use of (3.3) and the identity

$$\mathbf{v} \cdot \text{grad} \mathbf{v} = \text{grad}(\mathbf{v}^2/2) - \mathbf{v} \times \text{curl} \mathbf{v}$$

in the Euler equation of motion:

$$\frac{\partial \mathbf{v}}{\partial t} + \mathbf{v} \cdot \text{grad} \mathbf{v} = \mathbf{F} - \frac{1}{\rho} \text{grad } p$$

with the body force \mathbf{F} given by the gravitational field $-\text{grad } \Omega$.

3.2 Geometry

The choice of coordinates is commonly determined by reference to the boundary, and the geometry associated with a curved boundary (the bed) is strictly speaking not Euclidean but *Riemannian*. Thus the (s, n) - coordinates adopted by Dressler (1978) lead to direct involvement of bed curvature (κ), characteristic of the differential geometry of the space.

Regarding the bed as a smooth two-dimensional Riemannian manifold R^2 , we may introduce Gaussian coordinates ξ^1, ξ^2 (generally non-orthogonal) with covariant symmetric metric surface tensor $a_{\alpha\beta}$ (see figure 3.1). The operations

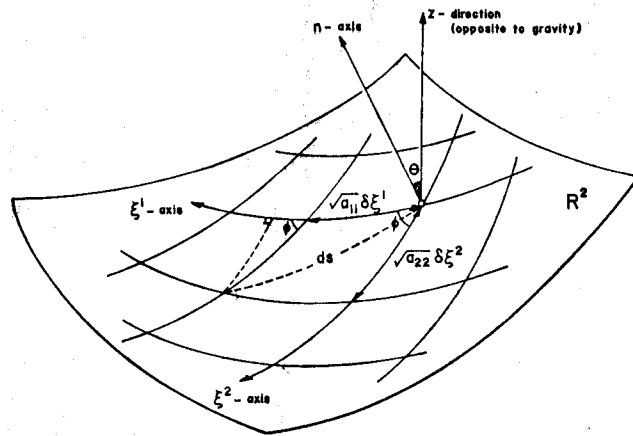


Figure 3.1 Geometry of the bed

$$ds^2 = (\sqrt{a_{11}} \delta \xi^1 + \sqrt{a_{22}} \delta \xi^2 \cos \phi)^2 + (\sqrt{a_{22}} \delta \xi^2 \sin \phi)^2 \\ = a_{\alpha\beta} \delta \xi^\alpha \delta \xi^\beta, \text{ where } a_{12} = a_{21} \equiv \sqrt{a_{11} a_{22}} \cos \phi.$$

² Greek indices are assigned to the surface and italic indices are assigned to the space; thus $\alpha, \beta \in \{1, 2\}$ and $i, j, k \in \{1, 2, 3\}$.

grad , div and curl in R^2 are (Kyrala, 1967):

$$\left. \begin{aligned} \text{grad}_2 \phi &= \phi_{, \alpha} \\ \text{div}_2 \mathbf{F} &= \frac{1}{\sqrt{a}} (\sqrt{a} F^\alpha)_{, \alpha} \\ \text{curl}_2 \mathbf{F} &= \frac{1}{\sqrt{a}} e^{\alpha\beta} F_{\beta, \alpha} \end{aligned} \right\} \quad (3.8)$$

where ϕ is a scalar field, F^α and F_α are the respective contravariant and covariant components of a surface vector³ \mathbf{F} , a denotes the determinant $|a_{\alpha\beta}|$, $e^{\alpha\beta}$ the usual completely antisymmetric double index symbol (of Levi-Civita), and $\partial/\partial \xi^\alpha$ is denoted by an α following a comma.

With coordinate n normally upwards from the bed so that $n=0$ is R^2 and $n=h(\xi^1, \xi^2, t)$ is the free surface of flow, the (ξ^1, ξ^2, n) - space⁴ is a three-dimensional Riemannian manifold R^3 with covariant symmetric metric space tensor

$$\{g_{ij}\} = \begin{pmatrix} J_1^2 a_{11} & J_1 J_2 a_{12} & 0 \\ J_2 J_1 a_{21} & J_2^2 a_{22} & 0 \\ 0 & 0 & 1 \end{pmatrix}, \quad (3.9)$$

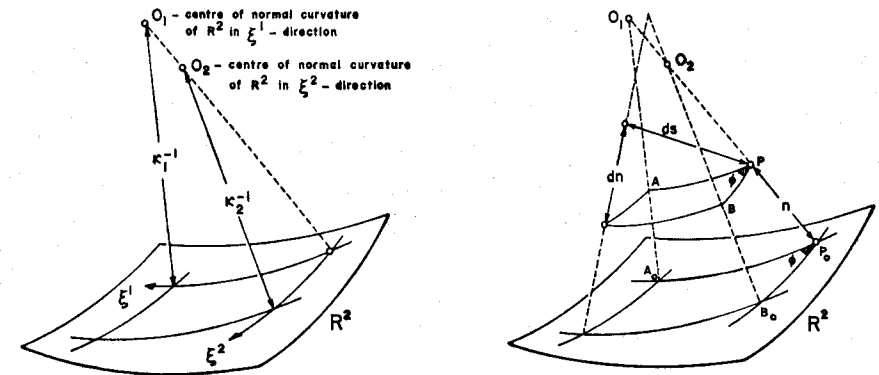


Figure 3.2 Geometry of the space

$$PA/P_0A_0 = J_1 \text{ and } PB/P_0B_0 = J_2, \quad ds^2 = g_{\alpha\beta} \delta \xi^\alpha \delta \xi^\beta + (\delta n)^2,$$

$$\text{where } \{g_{\alpha\beta}\} = \begin{pmatrix} J_1 & 0 \\ 0 & J_2 \end{pmatrix} \begin{pmatrix} a_{11} & a_{12} \\ a_{21} & a_{22} \end{pmatrix} \begin{pmatrix} J_1 & 0 \\ 0 & J_2 \end{pmatrix}$$

³ A surface vector at any point P on the surface is any vector on the tangent plane to the surface at P .

⁴ Whenever $\kappa_1 > 0$ or $\kappa_2 > 0$, the condition for unique representation of points in the flow domain by the normal coordinate n is $n < \min\{\kappa_1^{-1}, \kappa_2^{-1}\}$.

where

$$J_{\alpha}(\xi^1, \xi^2, n) \equiv 1 - \kappa_{\alpha} n \quad (3.10)$$

and $\kappa_{\alpha}(\xi^1, \xi^2)$ denotes the *normal curvature* of R^2 in the ξ^{α} -direction (c.f. figure 3.2). In R^3 , we recall the well known formulae (Kyrälä, 1967)

$$\left. \begin{aligned} \text{grad}_3 \phi &= \phi_{,i} \\ \text{div}_3 \mathbf{v} &= \frac{1}{\sqrt{g}} (\sqrt{g} v^i)_{,i} \\ \text{curl}_3 \mathbf{v} &= \frac{1}{\sqrt{g}} e^{ijk} v_{k,j} \end{aligned} \right\} \quad (3.11)$$

where v^i and v_i are the respective contravariant and covariant components of a space vector \mathbf{v} , g denotes the determinant $|g_{ij}|$, and e^{ijk} the usual completely antisymmetric triple index symbol (of Levi-Civita). Further, from (3.9)

$$\sqrt{g} = J_1 J_2 \sqrt{a}. \quad (3.12)$$

Moreover, if we define the covariant symmetric tensor

$$\{g_{\alpha\beta}\} \equiv \begin{pmatrix} J_1^2 a_{11} & J_1 J_2 a_{12} \\ J_2 J_1 a_{21} & J_2^2 a_{22} \end{pmatrix} \quad (3.13)$$

the associated contravariant tensor (defined by $g^{\alpha\beta} g_{\beta\gamma} = \delta_{\gamma}^{\alpha}$) is

$$\{g^{\alpha\beta}\} \equiv \begin{pmatrix} \frac{1}{J_1^2} \frac{a_{22}}{a} & -\frac{1}{J_1 J_2} \frac{a_{12}}{a} \\ -\frac{1}{J_2 J_1} \frac{a_{21}}{a} & \frac{1}{J_2^2} \frac{a_{11}}{a} \end{pmatrix} \quad (3.14)$$

and at the bed ($n=0$)

$$g_{\alpha\beta 0} = a_{\alpha\beta} \quad \text{and} \quad g^{\alpha\beta}_0 = a^{\alpha\beta}, \quad (3.15)$$

where $a^{\alpha\beta}$ is the associated contravariant metric surface tensor of R^2 .

Hence the fundamental equations may be re-written

$$\frac{\partial}{\partial \xi^{\alpha}} \{J_1 J_2 \sqrt{a} g^{\alpha\beta} v_{\beta}\} + \frac{\partial}{\partial n} \{J_1 J_2 \sqrt{a} w\} = 0 \quad (3.1)*$$

$$\left\{ \begin{aligned} \frac{\partial v^{\alpha}}{\partial t} + g \frac{\partial E}{\partial \xi^{\alpha}} &= 0 \\ \frac{\partial w}{\partial t} + g \frac{\partial E}{\partial n} &= 0 \end{aligned} \right. \quad (3.2\alpha)* \quad (3.2n)*$$

$$\left\{ \begin{aligned} \frac{\partial v^{\alpha}}{\partial n} - \frac{\partial w}{\partial \xi^{\alpha}} &= 0 \\ \frac{\partial v_2}{\partial \xi^1} - \frac{\partial v_1}{\partial \xi^2} &= 0 \end{aligned} \right. \quad (3.3\alpha)* \quad (3.3n)*$$

$$\frac{\partial h}{\partial t} + v^{\alpha}_h \frac{\partial h}{\partial \xi^{\alpha}} = w_h \quad (3.4)*$$

$$w_h = 0 \quad (3.5)*$$

$$p_h = \Pi \quad (3.6)*$$

where $\Omega = g\mathbf{z} = g(\zeta + n \cos \theta)$, and

$$E \equiv \zeta + n \cos \theta + \frac{p}{\rho g} + \frac{g^{\alpha\beta} v_{\alpha} v_{\beta} + w^2}{2g} \quad (3.7)*$$

Here θ denotes the angle n makes with z (c.f. figure 3.3); (v^1, v^2, w) and (v_1, v_2, w) are respectively the contravariant and covariant components of the flow velocity \mathbf{v} (a space vector).

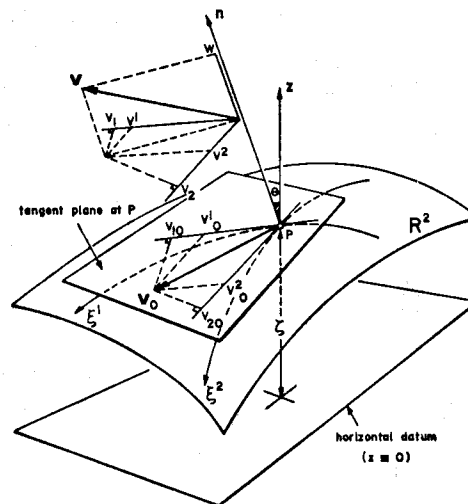


Figure 3.3 Flow over a curved bed

3.3 Shallow-Flow Assumptions

For shallow-flow it is assumed that the normal length scale (n -direction) relative to the characteristic length (ξ^α -direction) is small. One can infer from continuity (3.1)* that $|w| \ll |v^\alpha|$, so that in terms of a "tag" $\epsilon \ll 1$ the terms in the fundamental equations are ordered as tabulated below.

	ξ^α	n	h	E	v^α, v_α	w
$\frac{\partial}{\partial t}, \frac{\partial}{\partial \xi^\alpha}$	1	ϵ	ϵ	1	1	ϵ
$\frac{\partial}{\partial n}$			ϵ	1	1	ϵ
				ϵ^{-1}	ϵ^{-1}	1

(3.16)

The following alternative approach to the shallow-flow approximation has been widely used by hydraulic engineers in the study of open channel flow (Wehausen and Laitone, 1960). Here it is essential to nondimensionalize the variables so that the vertical (n) and the horizontal (s) distances are stretched by different amounts. Let L be a scale for horizontal measurement and H one for the vertical measurement. Defining a "shallowness parameter" $\sigma \equiv (H/L)^2$ and introducing new nondimensional variables $\tilde{s}, \tilde{n}, \dots$ by the equations

$$\begin{aligned} \tilde{s} &= s\sqrt{\sigma} & \tilde{v} &= v/\sqrt{g} & \tilde{E} &= E\sqrt{\sigma} \\ \tilde{n} &= n & \tilde{w} &= w\sqrt{\sigma/g} & \tilde{h} &= h \\ \tilde{t} &= t\sqrt{g\sigma} & \tilde{p} &= p/\rho g \end{aligned}$$

we can arrive at the same conclusion as (3.16) regarding the relative order of magnitude of terms in the fundamental equations. This ordering is of course the initial step of the asymptotic derivation given by Dressler (1978) for plane shallow-flow over a curved bed (c.f. figure 2.4).

3.4 General Shallow-Flow Equations

Using (3.16), neglecting $O(\epsilon^1)$ terms with respect to $O(\epsilon^j)$ for $i-j \geq 2$, the fundamental equations reduce to the general shallow-flow equations:

$$(J_1 J_2)_h \frac{\partial h}{\partial t} + \text{div}_2 \mathbf{G} \mathbf{v}_0 = 0 \quad (3.17)$$

$$\frac{\partial \mathbf{v}_0}{\partial t} + \text{grad}_2 (gE) = \mathbf{0} \quad (3.18)$$

$$\text{curl}_2^T \mathbf{v}_0 = \mathbf{0} \quad (3.19)$$

where

$$E(\xi^1, \xi^2, t) \equiv \zeta + h \cos \theta + \frac{p_h}{\rho g} + g^{\alpha\beta} \frac{v_{\alpha 0} v_{\beta 0}}{2g} \quad (3.20)$$

$$v_\alpha(\xi^1, \xi^2, n, t) = v_{\alpha 0}(\xi^1, \xi^2, t) \quad (3.21)$$

$$w(\xi^1, \xi^2, n, t) = -\frac{1}{J_1 J_2} \text{div}_2 \mathbf{G} \mathbf{v}_0 \quad (3.22)$$

$$\frac{p(\xi^1, \xi^2, n, t) - p_h}{\rho g} = (h-n) \cos \theta + \{g^{\alpha\beta}_h - g^{\alpha\beta}\} \frac{v_{\alpha 0} v_{\beta 0}}{2g} \quad (3.23)$$

and

$$\mathbf{G} = \{G^{\alpha\beta}\} \equiv \left\{ \int_0^n J_1 J_2 g^{\alpha\beta} dn \right\} \equiv \begin{pmatrix} \frac{a_{22}}{a} \int_0^n \frac{J_2}{J_1} dn & -n \frac{a_{12}}{a} \\ -n \frac{a_{21}}{a} & \frac{a_{11}}{a} \int_0^n \frac{J_1}{J_2} dn \end{pmatrix}. \quad (3.24)$$

For shallow-flow, (3.2n)* and (3.3a)* imply that the total energy head E and the covariant space velocity components v_1, v_2 are uniform across the flow depth - i.e. $E = E(\xi^1, \xi^2, t) = E_h$ and $v_\alpha = v_{\alpha 0}(\xi^1, \xi^2, t)$.

From (3.1)*, (3.5)* and (3.21) we get (3.22); and since E is independent of n from (3.21) we get (3.23). In deriving (3.17) we integrate (3.1)* over the flow depth using (3.21) to get

$$\begin{aligned} -\{J_1 J_2 \sqrt{a} w\}_0^h &= \int_0^h \frac{\partial}{\partial \xi^\alpha} \{J_1 J_2 \sqrt{a} g^{\alpha\beta} v_\beta\} dn \\ &= \frac{\partial}{\partial \xi^\alpha} \sqrt{a} \left[\int_0^h J_1 J_2 g^{\alpha\beta} dn \right] v_{\beta 0} - \{J_1 J_2 \sqrt{a} v^\alpha\}_h \frac{\partial h}{\partial \xi^\alpha} \end{aligned}$$

and then invoke the kinematic boundary conditions at the bed and free surface (viz. (3.5)* and (3.4)*). Equations (3.18) and (3.19) follow immediately from (3.2a)* and (3.3n)* respectively, on using (3.21).

We now show that both Saint-Venant and Dressler equations are special cases of these general shallow-flow equations.

3.5 Special Cases

3.5A Saint-Venant Equations

Saint-Venant equations describe plane shallow-flow over a flat bed (c.f. figure 3.4). In this Euclidean limit $\kappa_1 \equiv \kappa_2 \equiv 0$ and, for Cartesian coordinates x, y on R^2 , $a_{\alpha\beta} = \delta_{\alpha\beta}$; thus the Jacobian $J_\alpha \equiv 1$, the metric tensor $g_{\alpha\beta} = \delta_{\alpha\beta}$, and $G^{\alpha\beta} \equiv \delta^{\alpha\beta}$.

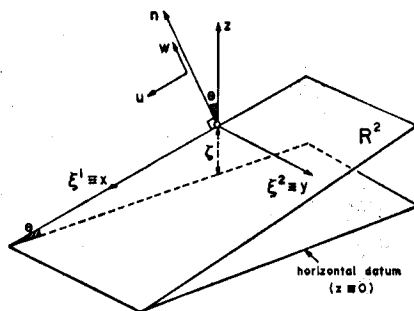


Figure 3.4 Definition sketch:
Saint-Venant equations

Since $\mathbf{V} = (u, 0, w)$, the shallow-flow equations are

$$\frac{\partial h}{\partial t} + \frac{\partial}{\partial x}(hu) = 0, \quad [\text{c.f. (2.1)}]$$

$$\left. \begin{aligned} \frac{\partial u}{\partial t} + g \frac{\partial E}{\partial x} &= 0, \\ E(x, t) &\equiv \zeta + h \cos \theta + \frac{p_h}{\rho g} + \frac{u^2}{2g}, \end{aligned} \right\} \quad [\text{c.f. (2.2)}]$$

where

$$u(x, n, t) = v_{10}(x, t),$$

$$w(x, n, t) = -n \frac{\partial u}{\partial x}$$

and

$$\frac{p(x, n, t) - p_h}{\rho g} = (h-n) \cos \theta : \text{hydrostatic.}$$

3.5B Dressler Equations

Dressler equations describe plane shallow-flow over a curved bed (c.f. figure 3.5). Orienting the axes as shown we have $\kappa_1 \equiv \kappa$ and $\kappa_2 \equiv 0$, and with arc lengths s, r measured orthogonally on R^2 : $a_{\alpha\beta} = \delta_{\alpha\beta}$. The Jacobian $J = 1 - \kappa n$,

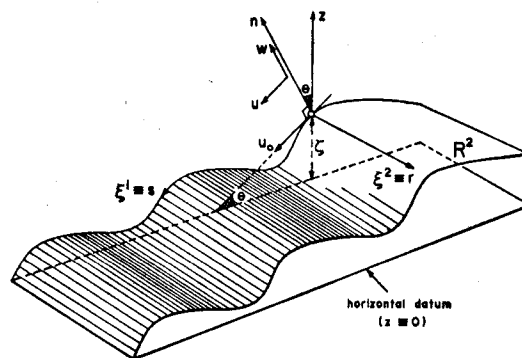


Figure 3.5 Definition sketch:
Dressler equations

$$\text{the metric tensor } \{g_{\alpha\beta}\} = \begin{pmatrix} J^2 & 0 \\ 0 & 1 \end{pmatrix}, \text{ and } \{G^{\alpha\beta}\} = \begin{pmatrix} -\frac{1}{\kappa} \ln J & 0 \\ 0 & n \left(1 - \frac{\kappa n}{2}\right) \end{pmatrix}.$$

Noting that the physical, the contravariant and the covariant components of the velocity \mathbf{V} are related by

$$\mathbf{V} = (u, 0, w) = (Jv^1, 0, w) = (v_1/J, 0, w),$$

and at the bed

$$u_0 = v^1_0 = v_{10},$$

the shallow-flow equations are

$$J_h \frac{\partial h}{\partial t} + \frac{\partial}{\partial s} \left(-\frac{u_0}{\kappa} \ln J_h \right) = 0, \quad [\text{c.f. (2.11)}] \quad (3.25)$$

$$\left. \begin{aligned} \frac{\partial u_0}{\partial t} + g \frac{\partial E}{\partial s} &= 0, \\ E(s, t) &\equiv \zeta + h \cos \theta + \frac{p_h}{\rho g} + J_h^{-2} \frac{u_0^2}{2g}, \end{aligned} \right\} \quad [\text{c.f. (2.7)}] \quad (3.26)$$

where

$$u(s, n, t) = \frac{u_0(s, t)}{J}, \quad (3.27)$$

$$\begin{aligned} w(s, n, t) &= \frac{1}{J} \frac{\partial}{\partial s} \left(\frac{u_0}{\kappa} \ln J \right) \\ &= \left(\frac{\ln J}{J\kappa} \right) \frac{\partial u_0}{\partial s} - \frac{1}{\kappa^2} \frac{d\kappa}{ds} \left(\frac{\ln J}{J} + \frac{\kappa n}{J^2} \right) u_0 \end{aligned} \quad (3.28)$$

and

$$\frac{p(s, n, t) - p_h}{\rho g} = (h-n) \cos \theta + [J_h^{-2} - J^{-2}] \frac{u_0^2}{2g} \quad (3.29)$$

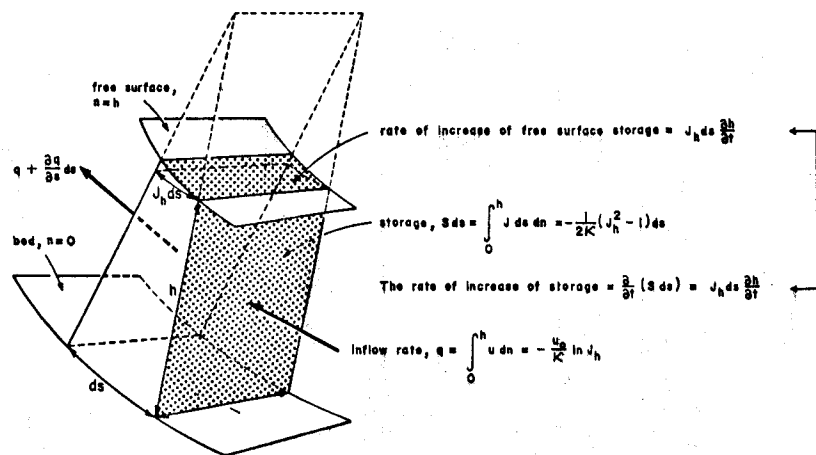


Figure 3.6 Mass conservation: $\frac{\partial S}{\partial t} + \frac{\partial q}{\partial s} = 0$

NOTES: 1 Equation (3.25) defines mass conservation for unit channel width—c.f. figure 3.6.

2 Equation (3.26) is a more compact form of Dressler's momentum equation (2.7), and displays the relation with energy.

3 Equation (3.27) may be re-written

$$(R-n)pu = Rpu_0$$

where $R \equiv \kappa^{-1}$ is radius of curvature—thus angular momentum about the local centre of curvature is constant.

3.6 Generalized Froude Number

The characteristics of Dressler equations (2.6) and (2.7) are defined by⁵

$$\frac{ds}{dt} = \frac{u_0}{(1-\chi)^2} \pm \sqrt{-\frac{\ln(1-\chi)}{(1-\chi)\kappa} \left[g \cos \theta + \frac{\kappa u_0^2}{(1-\chi)^3} \right]}, \quad (3.30)$$

where $\chi \equiv Kh$. Hence, for critical flow defined by $ds/dt \equiv 0$

⁵ Equations (2.6) and (2.7) can be written as

$$\frac{\partial \mathbf{r}}{\partial s} \mathbf{S} + \frac{\partial \mathbf{r}}{\partial t} \mathbf{T} = \mathbf{f}, \text{ where } \mathbf{r} = (h, u_0), \mathbf{S} = \begin{pmatrix} a & b \\ c & a \end{pmatrix} \text{ and } \mathbf{T} = \begin{pmatrix} 1 & 0 \\ 0 & 1 \end{pmatrix}.$$

Noting that $\frac{\partial \mathbf{r}}{\partial s} ds + \frac{\partial \mathbf{r}}{\partial t} dt = d\mathbf{r}$, the real eigenvalues given by $\left| \frac{\mathbf{S}}{ds} - \frac{\mathbf{T}}{dt} \right| = 0$,

i.e. $\frac{ds}{dt} = a \pm \sqrt{bc}$, correspond to the characteristic directions.

$$\left| \frac{u_0}{(1-\chi)^2} \right| = \left| \sqrt{-\frac{\ln(1-\chi)}{(1-\chi)\kappa} \left[g \cos \theta + \frac{\kappa u_0^2}{(1-\chi)^3} \right]} \right|$$

$$\text{or } \frac{u_0^2}{gh \cos \theta} = -\frac{(1-\chi)^3 \ln(1-\chi)}{\chi [1 + \ln(1-\chi)]}. \quad (3.31)$$

Dressler (1978) defined the left member as the *local Froude number* f and identified the right member as the *local critical Froude number* f_c .

Recalling that $u_h = u_0/(1-\chi)$, (3.31) can be re-written as

$$u_h^2 = c^2, \quad (3.32)$$

$$\text{where } c \equiv \sqrt{-\frac{(1-\chi) \ln(1-\chi)}{\chi [1 + \ln(1-\chi)]} gh \cos \theta} \quad (3.33)$$

is identifiable as the *celerity* (i.e. the speed of small disturbances at the free surface) in *curved bed flow*, and clearly as $\kappa \rightarrow 0$ (flat bed) the known result $c = \sqrt{gh \cos \theta}$ is recovered.⁶

Thus at the critical flow, any small disturbance at the free surface travels with the same fluid particles. One may therefore preserve the definition of Froude number, originally introduced for flow over flat beds ($\kappa = 0$), as the ratio of free surface speed to celerity

$$F \equiv |u_h|/c, \quad (3.34)$$

which is 1 for critical flow irrespective of bed curvature; we recall that the flow is *subcritical/supercritical* according as $F \leq 1$. From (3.31) note that

$$F = \sqrt{f/f_c}. \quad (3.35)$$

3.7 Validity of the Dressler Equations

The singularity in the celerity (c.f. (3.33)) occurring where $1 + \ln(1-\chi) = 0$ or $\chi = 1 - e^{-1} \approx 0.6321$ defines an *absolute upper bound* $\chi_u = 0.6321$ for validity of the Dressler equations. Dressler (1978) suggested $\chi_u = 0.5$ and lower bound $\chi_l = -0.85$ (c.f. (2.13)). Within (χ_l, χ_u) any small disturbance at the free surface spreads faster over a concave bed ($\kappa > 0$), and slower over a convex bed ($\kappa < 0$), than over a flat bed ($\kappa = 0$)—c.f. figure 3.7.

The shallow-flow approximation of the fundamental equations (3.1) to (3.7) due to Dressler (1978) is first order, and in theory could be extended to higher order to extend the range of validity. Experimental verification of

⁶ Eliminating $g \cos \theta$ in (3.30) using (3.33), we get

$$\frac{ds}{dt} = \frac{u_h}{1-\chi} \pm \frac{c}{1-\chi} \sqrt{1 + (1 - F^2) \ln(1-\chi)},$$

which in the flat bed limit ($\kappa \rightarrow 0$) reduces to the well known result associated with the Saint-Venant equations— $ds/dt = u_h \pm \sqrt{gh \cos \theta}$.

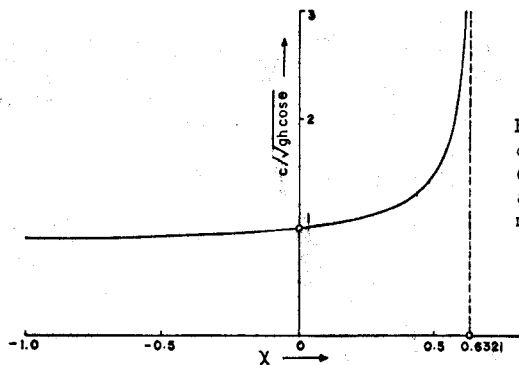


Figure 3.7 "Relative celerity" $c/\sqrt{gh \cos \theta}$ versus dimensionless curvature χ . (The curve is imaginary for $\chi > 0.6321$, and has minimum 0.8776 at $\chi = -5.0091$.)

the Dressler equations for *steady flow* is considered in subsequent chapters.

For *steady flow* we note that the *kinematic boundary condition* (3.4)

$$\frac{\partial h}{\partial t} + \frac{u_h}{J_h} \frac{\partial h}{\partial s} = w_h$$

expressed as

$$\frac{w}{u}|_h = \frac{1}{J_h} \frac{dh}{ds}$$

implies

$$|dh| \ll |J_h ds| \quad (3.36)$$

under the *shallow-flow assumption* $|w| \ll |u|$, (3.16). It is clear that (3.36) is more readily satisfied for *convex beds* ($\kappa < 0$) as h increases — c.f. figure 3.8.

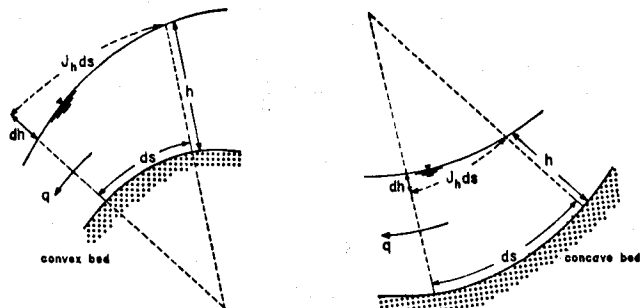


Figure 3.8 Geometrical interpretation of $|dh| \ll |J_h ds|$

IV STEADY SOLUTIONS OF THE DRESSLER EQUATIONS

Steady flow solutions of the Dressler equations are considered in this Chapter. Subcritical, critical and supercritical solutions exist and the location of the critical flow is identified. Flow stability is discussed, and the transition profile derived. Finally, application of the theory to flow over a tested spillway is described.

4.1 Steady Flow

For steady flow, (3.25) and (3.26) with $p_h \equiv 0$ reduce to

$$q \equiv -\frac{u_0}{\kappa} \ln(1-\kappa h) = \text{constant} \quad (4.1)$$

$$E \equiv \zeta + h \cos \theta + \frac{u_0^2}{2g} (1-\kappa h)^{-2} = \text{constant}, \quad (4.2)$$

so that eliminating u_0 gives the equation for the free surface (defined by h)

$$E = \zeta + h \cos \theta + \frac{q^2 \kappa^2}{2g} [(1-\kappa h) \ln(1-\kappa h)]^{-2} \quad (4.3)$$

or

$$\gamma(\chi) = \alpha + \beta \chi, \quad (4.4)$$

where

$$\left. \begin{aligned} \alpha &\equiv 2g(E - \zeta) / (q\kappa)^2 \\ \beta &\equiv -2g \cos \theta / (q^2 \kappa^3) \\ \chi &\equiv \kappa h \end{aligned} \right\} \quad (4.5)$$

and $\gamma(\chi) \equiv [(1-\chi) \ln(1-\chi)]^{-2}$.

The graphical solution of (4.4) is sketched in figure 4.1, and is interpreted as follows.

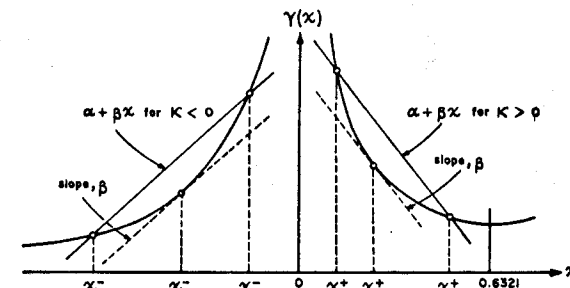


Figure 4.1 Solution of $\gamma(\chi) = \alpha + \beta\chi$

$$\text{Theorem(1)} \quad F \leq 1 \leftrightarrow |\gamma'(\chi)| \leq |\beta|. \quad (4.6)$$

To prove this we recall (3.31) and (3.35); using (4.1) to eliminate u_0

$$\begin{aligned} \bar{f} \leq \bar{f}_c &\leftrightarrow \frac{[-\kappa g / \ln(1-\chi)]^2}{gh \cos \theta} \leq -\frac{(1-\chi)^3 \ln(1-\chi)}{\chi [1 + \ln(1-\chi)]} \\ \text{or} \quad \frac{2g \cos \theta}{q^2 \kappa^3} \chi &\leq -\frac{2[1 + \ln(1-\chi)]}{[(1-\chi) \ln(1-\chi)]^3} \chi. \end{aligned}$$

Comparing with (4.5), we get

$$\bar{f} \leq \bar{f}_c \leftrightarrow -\beta \chi \leq -\gamma'(\chi) \chi.$$

Therefore, when

$$\left. \begin{aligned} \chi > 0 : \bar{f} \leq \bar{f}_c &\leftrightarrow -\beta \geq -\gamma'(\chi) \\ \chi < 0 : \bar{f} \leq \bar{f}_c &\leftrightarrow \beta \geq \gamma'(\chi) \end{aligned} \right\} \leftrightarrow |\beta| \geq |\gamma'(\chi)|; \text{ QED.}$$

Hence in figure 4.1 we identify the roots

$$\begin{aligned} \chi^-, \chi^+ &\rightarrow \text{subcritical flow} \\ \chi_c^-, \chi_c^+ &\rightarrow \text{critical flow} \\ \chi_0^-, \chi_0^+ &\rightarrow \text{supercritical flow} \end{aligned}$$

Note that

$$F^2 = \left(\frac{u}{c}\right)^2 = \frac{\bar{f}}{\bar{f}_c} = \frac{\gamma'(\chi)}{\beta} = \frac{2}{\beta} \frac{1 + \ln(1-\chi)}{[(1-\chi) \ln(1-\chi)]^3} \quad (4.7)$$

Differentiating (4.3) with respect to the horizontal coordinate we have

$$\begin{aligned} \frac{dE}{dx} &= \frac{d}{dx} \left[\zeta + h \cos \theta + \frac{q^2 \kappa^2}{2g} \gamma(\chi) \right] \\ &= (1-\chi) \frac{d\zeta}{dx} + \frac{q^2 \kappa}{g} [\gamma(\chi) + \gamma'(\chi) \chi / 2] \frac{d\kappa}{dx} + \left[1 + \frac{q^2 \kappa^3}{2g \cos \theta} \gamma'(\chi) \right] \cos \theta \frac{dh}{dx} = 0, \quad (4.8) \end{aligned}$$

since $d\theta/dx = (d\theta/ds)/(dx/ds) = \kappa/\cos \theta$, $\tan \theta = d\zeta/dx$ and $\chi \equiv \kappa h$. Using (4.4), (4.5) and (4.7) this reduces to

$$\frac{dE}{dx} = (1-\chi) \frac{d\zeta}{dx} + \frac{q^2 \kappa}{g} [\alpha + (1 + F^2/2) \beta \chi] \frac{d\kappa}{dx} + (1 - F^2) \cos \theta \frac{dh}{dx} = 0. \quad (4.9)$$

The above equation relates $d\zeta/dx$, $d\kappa/dx$ and dh/dx , and implies:

Theorem(2) In ideal shallow-flow over bed profile $\zeta = \zeta(x)$, the critical flow normally occurs at a point defined by

$$(1-\chi) \frac{d\zeta}{dx} + \frac{q^2 \kappa}{g} (\alpha + 3\beta \chi/2) \frac{d\kappa}{dx} = 0, \quad (4.10)$$

where χ is given by (4.4).

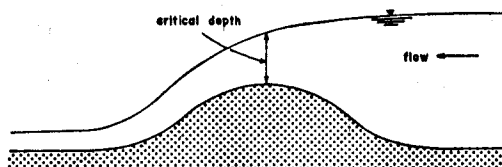


Figure 4.2 Symmetrical convex crest

NOTE: For symmetrical profiles $d\zeta/dx = d\kappa/dx = 0$ at the point of symmetry, where (4.10) is trivially satisfied.

At the critical section, from (4.7) $\beta = \gamma'(\chi)$ or

$$-\frac{2g \cos \theta}{q^2 \kappa^3} = \gamma'(\chi)$$

Hence, the discharge coefficient (excluding any viscous effect)

$$C_d \equiv \frac{q}{\sqrt{2g \cos \theta} h^{3/2}} = [\chi^3 \gamma'(\chi)]^{-1/2} = \sqrt{-\frac{[(1-\chi) \ln(1-\chi)]^3}{2\chi^3 [1 + \ln(1-\chi)]}} \quad (4.11)$$

For example, for $\kappa \rightarrow 0$: $C_d = 1/\sqrt{2} \approx 0.707$.

4.2 Stability

Since $\frac{dh}{dx} = \frac{1}{\kappa} \frac{d\chi}{dx} - \frac{\chi}{\kappa^2} \frac{d\kappa}{dx}$, from (4.9)

$$\frac{dE}{dx} = (1-\chi) \frac{d\zeta}{dx} + (1 - F^2) \frac{\cos \theta}{\kappa} \frac{d\chi}{dx} + \frac{q^2 \kappa}{g} \left[\alpha + (1 + F^2/2) \beta \chi - (1 - F^2) \cos \theta \frac{\beta \chi}{q^2 \kappa^3} \right] \frac{d\kappa}{dx},$$

or, recalling that $\frac{d\zeta}{ds} = \sin \theta$, $-\frac{2g \cos \theta}{q^2 \kappa^3} \equiv \beta$ and $\frac{d}{ds} = \frac{d\theta}{ds} \frac{d}{d\theta} = \kappa \frac{d}{d\theta}$,

$$\frac{dE}{ds} = (1-\chi) \sin \theta + (1 - F^2) \cos \theta \frac{d\chi}{d\theta} + \frac{q^2 \kappa^2}{2g} (2\alpha + 3\beta \chi) \frac{d\kappa}{d\theta}. \quad (4.12)$$

In a steady flow with viscous dissipation the momentum equation is

$$\frac{dE}{ds} = -S_e, \quad (4.13)$$

where the energy slope S_e may be given by a generalized Chézy formula. Hence, from (4.12) and (4.13), we get the differential equation for the free surface

$$\frac{d\chi}{d\theta} = \frac{-S_e - (1-\chi) \sin \theta - \frac{q^2 \kappa^2}{2g} (2\alpha + 3\beta \chi) \frac{d\kappa}{d\theta}}{(1 - F^2) \cos \theta}. \quad (4.14)$$

When there is no dissipation ($S_e = 0$), the solution of (4.14) is of course (4.3).

To study the stability of flow, let us take the simplest case of frictionless flow over a constant curvature bed, when (4.14) reduces to

$$\frac{d\chi}{d\theta} = -\frac{(1-\chi)\sin\theta}{(1-F^2)\cos\theta}. \quad (4.15)$$

Let us introduce an independent variable λ (parameter) such that

$$\left. \begin{aligned} \frac{d\chi}{d\lambda} &= \Phi(\theta, \chi) \equiv -(1-\chi)\sin\theta, \\ \frac{d\theta}{d\lambda} &= \Psi(\theta, \chi) \equiv (1-F^2)\cos\theta = \cos\theta + \sigma \frac{1+\ln(1-\chi)}{[(1-\chi)\ln(1-\chi)]^3}, \end{aligned} \right\} \quad (4.16)$$

where $\sigma \equiv q^2 \kappa^3 / g$. The autonomous system (4.16) has a singular point $P(\theta_0 \equiv 0, \chi_0)$ defined by $\Phi(\theta_0, \chi_0) = \Psi(\theta_0, \chi_0) = 0$.

Expanding Φ and Ψ as Taylor series about P :

$$\begin{aligned} \Phi(\theta, \chi) &= \Phi(0, \chi_0) + \left(\frac{\partial \Phi}{\partial \theta}\right)_P \theta + \left(\frac{\partial \Phi}{\partial \chi}\right)_P (\chi - \chi_0) + \dots = -(1-\chi_0)\theta + \dots \\ \Psi(\theta, \chi) &= \Psi(0, \chi_0) + \left(\frac{\partial \Psi}{\partial \theta}\right)_P \theta + \left(\frac{\partial \Psi}{\partial \chi}\right)_P (\chi - \chi_0) + \dots = \sigma m^2 (1-\chi_0) (\chi - \chi_0) \end{aligned}$$

where

$$m^2 (1-\chi_0) = \frac{1}{\sigma} \left(\frac{\partial \Psi}{\partial \chi}\right)_P = 3 \frac{\left[\ln(1-\chi_0) + \frac{25}{36}\right]^2 + \frac{11}{36}}{[(1-\chi_0)\ln(1-\chi_0)]^4} > 0. \quad (4.17)$$

The integral curves of (4.16) define the free surface, and their nature in the vicinity of the singular point P can be determined from the approximate linear system:

$$\left. \begin{aligned} \frac{d\chi}{d\lambda} &= -(1-\chi_0)\theta, \\ \frac{d\theta}{d\lambda} &= \sigma m^2 (1-\chi_0) (\chi - \chi_0); \end{aligned} \right\} \quad (4.18)$$

thus

$$(1-\chi_0) d\lambda = -\frac{d\chi}{\theta} = \frac{d\theta}{\sigma m^2 (\chi - \chi_0)}$$

or

$$\theta d\theta + \sigma m^2 (\chi - \chi_0) d\chi = 0,$$

whence

$$\theta^2 + \sigma m^2 (\chi - \chi_0)^2 = \text{constant}. \quad (4.19)$$

The integral curves are thus *ellipses* when $\sigma > 0$ (i.e. $\kappa > 0$) and *hyperbolae* when $\sigma < 0$ (i.e. $\kappa < 0$).

NOTES: 1 Concave Bed

When $\kappa > 0$, the singular point of the approximate linear system (4.18) is a *centre* (also called *vortex*); hence, is either a centre or a *focus* for the original autonomous system (4.16). But $d\chi/d\theta = \Phi/\Psi$ has an integral (given by $\gamma(\chi) = \alpha + \beta\chi$), therefore the singular point of the original autonomous system is a *centre* and *weakly stable* (Plaat, 1971).

2 Convex Bed

When $\kappa < 0$, the singular point is a *saddle* and always *unstable*.

- 3 At the singular point P , $\Psi(\theta, \chi) = 0$; hence, from (4.16) $F=1$ —i.e. the flow is *critical* at P and $\chi_0 = \chi_c^-$ or χ_c^+ .

4.3 Transition Profile

In (4.8), writing derivatives with respect to s rather than x , and noting that $d\zeta/ds = \sin\theta$ and $dE/ds = -S_e$, we get the *backwater curve* for flow over curved beds:

$$\frac{dh}{ds} = -(1-\chi) \tan\theta \frac{1-(q/q_n)^2}{1-(q/q_c)^2}, \quad (4.20)$$

where the *quasi-normal discharge* q_n , and the *critical discharge* q_c are given by

$$q_n^2 \equiv \frac{-(1-\chi)\sin\theta}{\frac{S_e}{q^2} + \frac{\kappa}{2g}[2\gamma(\chi) + \gamma'(\chi)\chi] \frac{d\kappa}{ds}}, \quad (4.21)$$

$$q_c^2 \equiv \frac{-2g\cos\theta}{\kappa^3 \gamma'(\chi)}. \quad (4.22)$$

In the flat bed limit ($\kappa \rightarrow 0$)

$$S_e/q^2 \rightarrow 1/(C^2 h^3), \quad (C : \text{Chézy coefficient})$$

$$\kappa^3 \gamma'(\chi) \rightarrow -2/h^3$$

so that

$$\left. \begin{aligned} q_n^2 &\rightarrow -C^2 h_0^3 \sin\theta, \\ q_c^2 &\rightarrow g h_c^3 \cos\theta, \end{aligned} \right\} \quad (4.23)$$

where h_0 and h_c denote respectively the *normal* and the *critical depths* for flat bed channel flow.

The *transition profile* is the locus of the transition points defined by $q_n = q_c$ (Escoffier, 1958); that is

$$\frac{S_e}{q^2} + \frac{\kappa}{2g}[2\gamma(\chi) + \gamma'(\chi)\chi] \frac{d\kappa}{ds} = \frac{-2g\cos\theta}{\kappa^3 \gamma'(\chi)},$$

or

$$T(\chi) = m(x) + \varepsilon(x, \chi) \frac{S_e}{q^2} \quad (4.24)$$

where, on using $\gamma(\chi) \equiv [(1-\chi)\ln(1-\chi)]^{-2}$, $d\theta/ds = \kappa$, and $dx/ds = \cos\theta$ and $\kappa = (d^2\zeta/dx^2)\cos^3\theta$, we have

$$T(\chi) \equiv \frac{(1-\chi)\gamma'(\chi)}{[2\gamma(\chi) + \gamma'(\chi)\chi]} = \frac{(1-\chi)[1+\ln(1-\chi)]}{\chi + \ln(1-\chi)}, \quad (4.25a)$$

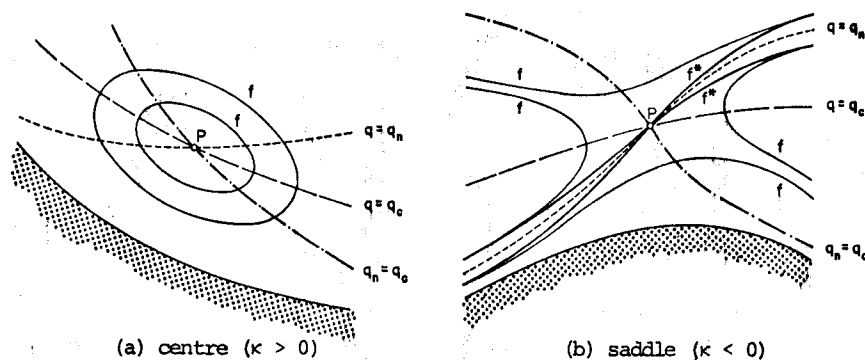


Figure 4.3 Flow profiles around a singular point f —flow profiles, f^* —flow profiles passing through P and asymptotic to $q = q_n$.

$$m(x) \equiv \frac{\cot \theta}{\kappa} \frac{d\kappa}{ds} = \frac{\zeta''' [1 + (\zeta')^2]}{\zeta' (\zeta'')^2} - 3, \quad (4.25b)$$

and

$$\epsilon(x, \chi) \equiv \frac{2g \cot \theta}{\kappa^3} [2\gamma(\chi) + \gamma'(\chi)\chi]^{-1} \quad (4.25c)$$

a prime (') in $m(x)$ denotes d/dx . Figure 4.3 depicts flow profiles around a singular point (c.f. section 4.2).

At a point where $d\zeta/dx = d\kappa/ds = 0$ the transition profile is not defined; however, in a frictionless flow the transition profile passes through the critical point (*Theorem(2)*).

The transition profile for a *frictionless flow* over the bed $\zeta(x)$ is given by ((4.24) with $S_b \equiv 0$)

$$T(\chi) = m(x). \quad (4.26)$$

From figure 4.4, note that (4.26) can be solved when $\kappa > 0$ only if $m < 0$, and when $\kappa < 0$ only if $m < -4.9108$.

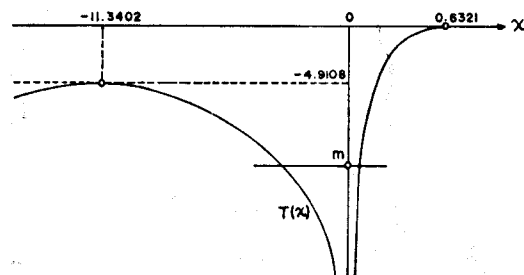


Figure 4.4 Sketch of the solution for $T(\chi) = m(x)$

4.4 Flow Over a Spillway Crest

We apply the shallow-flow equations with bed curvature to steady flow over a spillway crest. In dimensionless form (4.3) becomes

$$\left(\frac{E}{H_d} - \frac{\zeta}{H_d} \right) = \left(\frac{\cos \theta}{\kappa H_d} \right) \chi + F \left(\frac{\kappa H_d}{(1-\chi) \ln(1-\chi)} \right)^2, \quad (4.27)$$

where H_d denotes a reference head ("design head")

$$\chi \equiv \kappa h, \quad F \equiv \frac{q^2}{2gH_d^3}. \quad (4.28)$$

The dimensionless pressure head at the bed ($n=0$)

$$\frac{p_0}{\rho g H_d} = \left(\frac{E}{H_d} - \frac{\zeta}{H_d} \right) - F \left(\frac{\kappa H_d}{\ln(1-\chi)} \right)^2, \quad (4.29)$$

where p_0 denotes the pressure at the bed.

Chow (1959) has summarised model tests by the U.S. Army Engineers Waterways Experiment Station of so-called WES shapes for high overflow spillways. We consider the case of vertical upstream face without piers described in Section 14.6 of that book.

The spillway crest is given nondimensionally by

$$\frac{\zeta}{H_d} = -\frac{1}{2} \left(\frac{x}{H_d} \right)^{1.85} \quad (4.30)$$

and experimental coordinates of the upper nappe profile are given for dimensionless operating heads (excluding the velocity head) $H/H_d = 0.50, 1.00$ and 1.33 . We consider the nappe coordinate domain $0.2 < x_n/H_d < 1.8$, for which the ranges of χ are summarised in the table:

H/H_d	$\frac{x_n}{H_d} = 0.2$	$\frac{x_n}{H_d} = 1.8$
0.50	-0.320	-0.016
1.00	-0.745	-0.059
1.33	-1.029	-0.110

It is notable that $\chi < -0.85$ near the crest for $H/H_d = 1.33$, somewhat *outside* the tentative range of validity suggested by Dressler (1978) for experimental check of the equations.

Setting $E = H$, we calculated the values of the parameter F (related to the Froude number) in (4.27) to fit the experimental upper nappe profiles at the nine tabular points $x_n/H_d = 0.2(0.2)1.8$. The pointwise deviation of F

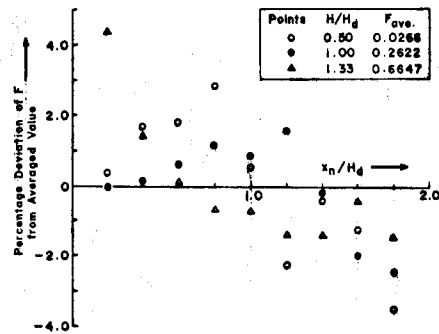


Figure 4.5 Pointwise percentage deviation of F

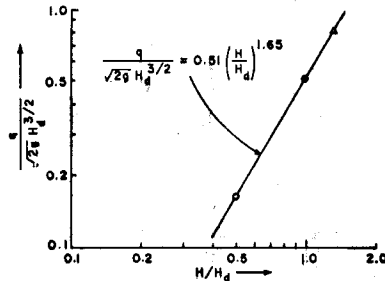


Figure 4.6 Discharge versus operating head

from its average value is not more than 4%, as shown in figure 4.5.⁷ The inferred dimensionless flows per unit width (\sqrt{F}) for operating heads $H/H_d = 0.50, 1.00$ and 1.33 are $0.163, 0.512$ and 0.815 ; weirs of simpler shapes are often used for flow measurements (see for example Ackers et al., 1978). Further, a logarithmic plot of averaged \sqrt{F} against operating head H/H_d shown in figure 4.6 yields the formula

$$\frac{q}{\sqrt{2g} H_d^{3/2}} = 0.51 \left(\frac{H}{H_d} \right)^{1.65} \quad (4.31)$$

$$\frac{q}{\sqrt{2g} H_d^{3/2}} = 0.51 \left(\frac{H}{H_d} \right)^{0.15} \quad (4.31)^*$$

Introducing a local Froude number as defined by Dressler (1978) viz.

$$\bar{F} \equiv \frac{u_0^2}{gh \cos \theta} \quad (4.32)$$

with $E = H$, (4.2) reads

$$H = \zeta + \left[1 + \frac{\bar{F}}{2(1-\chi)^2} \right] h \cos \theta$$

whence

$$\bar{F} = 2(1-\chi)^2 \left[\left(\frac{H}{H_d} - \frac{\zeta}{H_d} \right) \frac{KH_d}{\chi \cos \theta} - 1 \right] \quad (4.33)$$

⁷ Equation (4.27) defines the relation between $(E/H_d, F, \chi)$. To test this relation experimentally one must at least know either $(E/H_d, \chi)$ or (F, χ) . For instance, given the energy (E/H_d) and the spillway and nappe profiles (χ for different x), (4.27) defines F uniquely; energy loss due to the build up of a turbulent boundary layer as we go down from the crest accounts for any slight error trend in estimating F (c.f. figure 4.5). However, given either the energy or the flow (q), using (4.31) and (4.27) one can solve numerically for the unknown nappe.

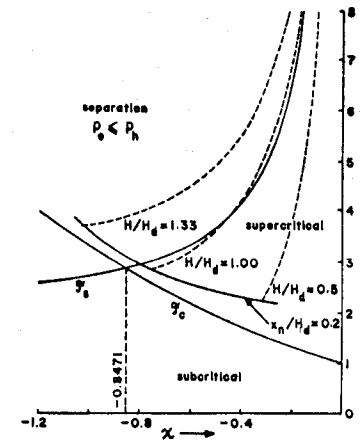


Figure 4.7 Curves for flow separation and critical flow

$$\bar{F}_s = -\frac{2(1-\chi)^2}{\chi(2-\chi)}$$

$$\bar{F}_c = -\frac{(1-\chi)^3 \ln(1-\chi)}{\chi [1 + \ln(1-\chi)]}$$

The local Froude number as a function of χ (shown in figure 4.7) corresponds to supercritical flow with or without separation.

Using the averaged values of F found from the upper nappe profiles, we computed theoretical pressure profiles from (4.29) for $H/H_d = 0.50, 1.00$ and 1.33 , to compare with the experimental profiles in the range $0 < x/H_d < 1.2$ reproduced in Chow (1959) figure 14-13: see figure 4.8. These experimental pressure profiles at the bed are affected by separation at larger heads and build up of local turbulence, particularly behind curvature discontinuities that should be avoided (Rouse and Reid, 1935) but are clearly indicated in Chow's figure. Slight modification of the results to allow for the influence of the neglected approach velocity head might be expected. We also fitted the experimental pressure profiles shown in Chow (1959) as best we could to (4.29), to obtain new parameter values $\sqrt{F}^* = 0.160, 0.507$ and 0.797 for the respective dimensionless operating heads $H/H_d = 0.50, 1.00$ and 1.33 : we obtained

$$\frac{q}{\sqrt{2g} H_d^{3/2}} = 0.50 \left(\frac{H}{H_d} \right)^{1.65}$$

4.5 Flow Over a Spillway Toe

Assuming negligible potential energy, various authors have given analytic solutions for steady ideal flow over a spillway toe. Douma (1954) and Balloffet (1961) used a "free-vortex" approximation, and Henderson and Tierney (1963) used a hodograph transformation to study irrotational flow for large curvature. A detailed discussion of their assumptions may be found in Henderson (1966) and also in Dobson (1967), who computed solutions by finite difference methods.

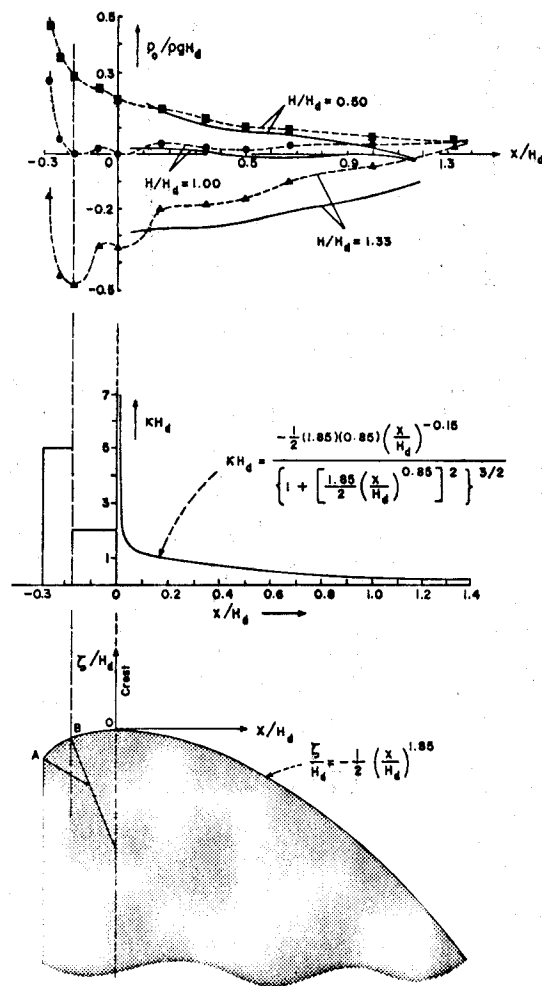


Figure 4.8 Pressure profiles along the spillway crest
 - - - tested spillway data (c.f. Chow, 1959)
 — theory

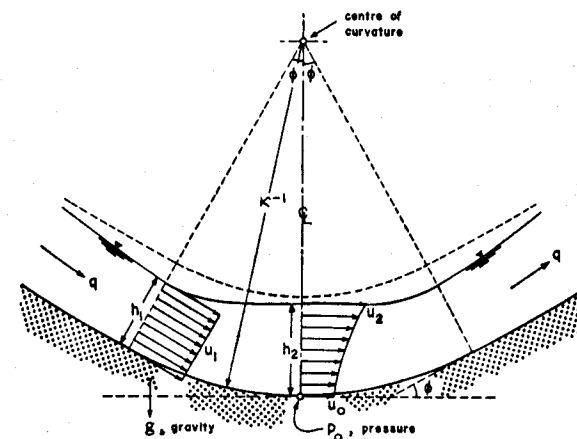


Figure 4.9 Flow at a spillway toe

The irrotational nature of the shallow-flow equations implicit in (3.27) leads to an identical solution if the potential energy is neglected. It follows from the *Bernoulli equation* (c.f. (3.7)* or (4.2)) that the particle speed at the free surface is constant (u_1 , say); hence from (4.1) and (3.29) we have the dimensionless curvature

$$\Omega^{-1} \equiv kh_1 = \Omega \ln \Omega^{-1} \quad (4.34)$$

and the pressure coefficient

$$C_p \equiv \frac{p_0}{\frac{1}{2} \rho u_1^2} = 1 - \Omega^2, \quad (4.35)$$

where $\Omega \equiv 1 - kh_2$, p_0 is the bed pressure at the point of symmetry, and h_1, h_2 are the initial and central depths respectively (c.f. figure 4.9). This solution is identical with that of "free-vortex" theory and is valid when $kh_1 \leq 1/6$ or $kh_2 \leq 0.185$ according to Henderson and Tierney (1963).

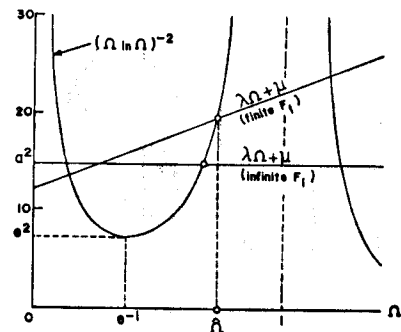
Of course the shallow-flow equations also readily permit a solution including the potential energy. In the symmetric case shown in figure 4.9 for example, it follows from (4.1) and (4.2) that

$$\frac{1}{(\Omega \ln \Omega)^2} = \lambda \Omega + \mu, \quad (4.36)$$

where $\lambda \equiv 2a^3 F_1^{-1}$, $\mu \equiv a^2 - 2a^2(a-1)F_1^{-1} \cos \phi$, $a \equiv (kh_1)^{-1}$ as before, and $F_1 \equiv u_1^2/(gh_1)$.

The bed pressure at the point of symmetry (p_0) now consists of a hydrostatic component

$$p_s = \rho gh_2$$

Figure 4.10 Root $\hat{\Omega}$ of equation (4.36)

and a centrifugal component

$$P_C = \frac{1}{2} \rho u_0^2 [(1 - \kappa h_2)^{-2} - 1],$$

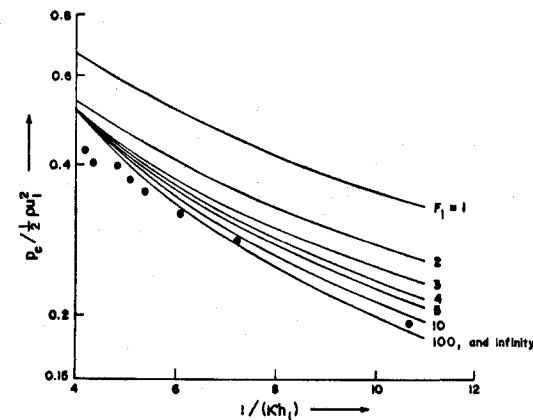
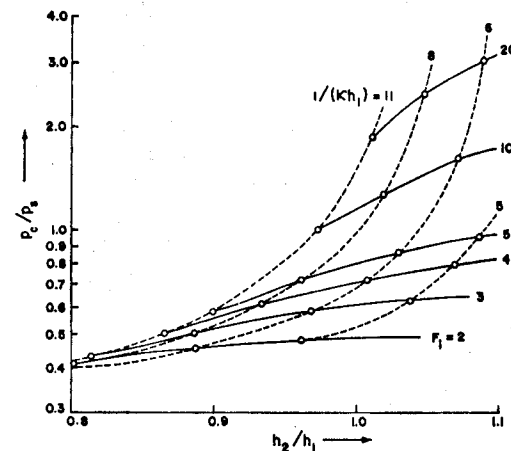
or correspondingly

$$C_S \equiv \frac{P_S}{\frac{1}{2} \rho u_1^2} = \frac{2a}{F_1} (1 - \Omega) \quad (4.37)$$

$$C_C \equiv \frac{P_C}{\frac{1}{2} \rho u_1^2} = (1 - \Omega^2) (a\Omega \ln \Omega)^{-2}. \quad (4.38)$$

When the potential energy is neglected ($F_1 \rightarrow \infty$) the hydrostatic part vanishes, so that $C_P = C_C$. The root $e^{-1} \leq \hat{\Omega} < 1$ of (4.36) that corresponds to the low potential energy limit (infinite Froude number) described above is shown in figure 4.10.⁸ Corresponding centrifugal pressure profiles for various Froude numbers are shown in figure 4.11, and we note that the bed pressure at the point of symmetry is increased when the potential energy is included. Thickening of the flow layer associated with increasing centrifugal pressure is illustrated in figure 4.12. We note that the solution validity is as before, and that we have continued to neglect surface disturbances that may occur at high Froude number.

⁸ Since $\chi \neq 1 - e^{-1}$ (≈ 0.6321), we have $\hat{\Omega} \equiv 1 - \chi \neq e^{-1}$

Figure 4.11 Maximum centrifugal pressure versus toe curvature, for $2\phi = 45^\circ$
• experiment by Henderson and Tierney (1963)Figure 4.12 Flow layer thickening with increasing centrifugal pressure, for $2\phi = 45^\circ$

V EXPERIMENT

The experimental setup to test the Dressler equations for steady flow is illustrated and the measurements made are outlined. The processing of experimental data to a form readily comparable with theoretical values is first described, before results for a symmetric and an unsymmetric profile are discussed.

5.1 Experimental Setup

The experimental setup is shown in figure 5.1. The experiments were carried out in a 915 cm × 75 cm × 44.5 cm flume made of a steel frame with glass windows on both vertical sides. The bed was elevated by 10 cm using 1.5 cm thick plywood, to house the plastic tubes connecting the piezometer tapplings along the centre line of the curved bed model (c.f. figure 5.2) and the piezometers. The flume width was vertically partitioned along the entire channel length into two compartments, again using 1.5 cm plywood. The larger compartment was 30 cm wide and served as the test channel for steady flow over curved bed models. The test section was at a distance of 366 cm from the inlet box. The bed pressure-piezometers were set up within the smaller compartment. The inflow to the inlet box through a 15.24 cm (6 in) dia. cast iron pipe was controlled by a gate valve.

The Dressler equations were examined for steady flow over two curved bed models, one a *symmetric profile* shaped after the normal distribution and the other an *unsymmetric profile* fashioned by B-Splines (c.f. Appendix-A). In each case the model was fabricated as described in figure 5.2.

5.2 Measurements

A Discharge, Q

A 7.26 cm (3 in) dia. orifice, placed well before the control valve in the 15.24 cm (6 in) dia. inflow pipe, was employed to rate the inflow. Because of rapid oscillation of the mercury column in the U-tube manometer attached to both sides of the orifice, about 25 readings of the simultaneous mercury levels in both legs of the manometer were recorded at about 10 sec. intervals to estimate the average mercury level difference H (cm). The accuracy of the manometer scale was 0.1 cm. The orifice equation (at 27°C)

$$Q = 30 \times 157.03 \sqrt{H} \text{ cm}^3/\text{s}. \quad (5.1)$$

was used to give the steady unit width discharge

$$q = Q/30 \text{ cm}^3/\text{s} \cdot \text{cm}. \quad (5.1)^*$$

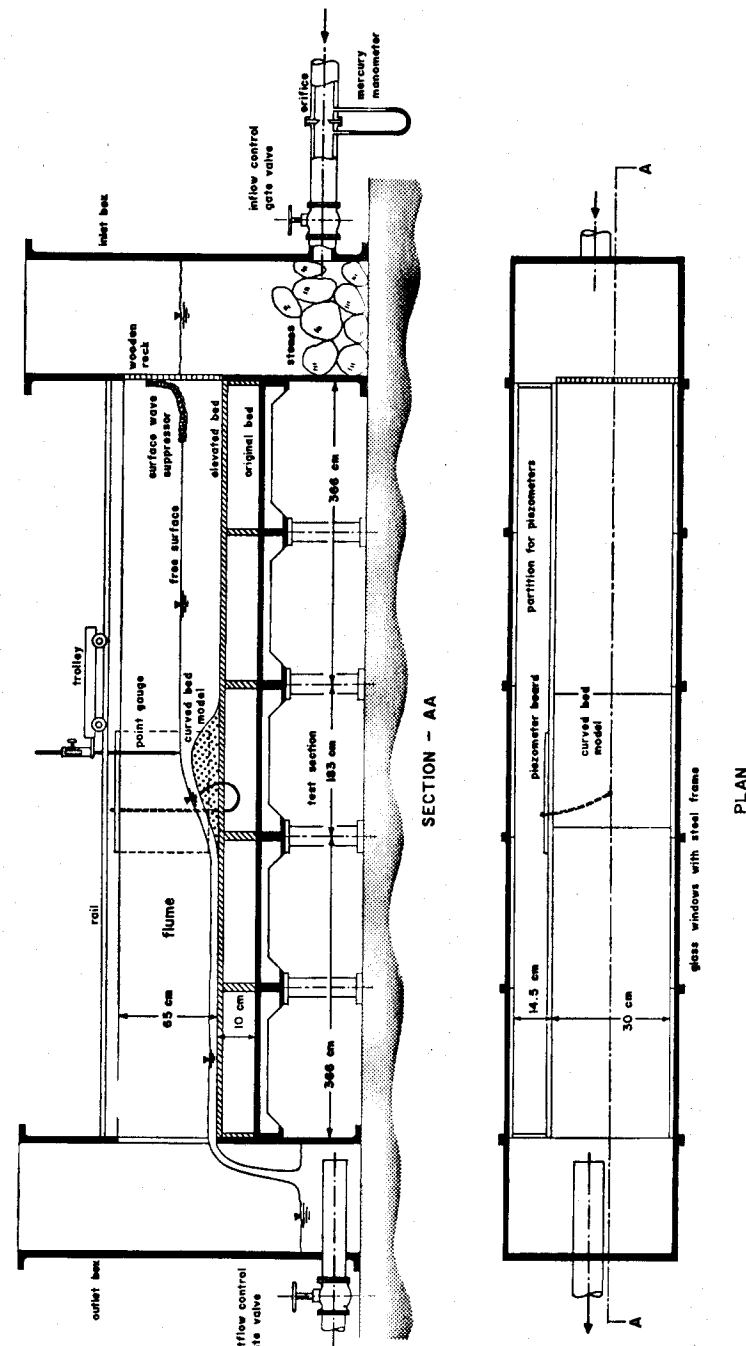


Figure 5.1 Experimental setup

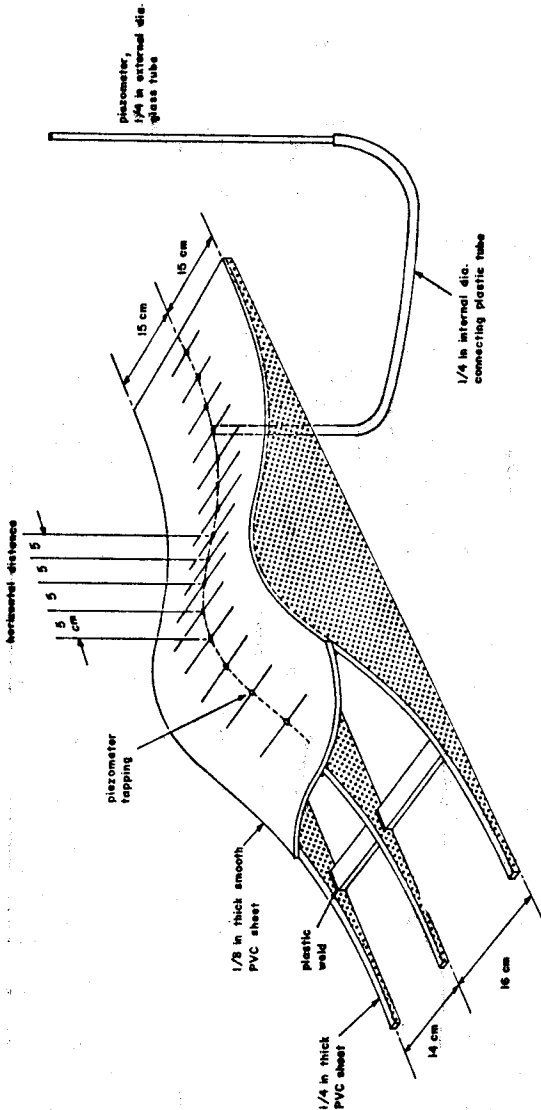


Figure 5.2 Dissection showing the construction of the curved bed

B Energy Head, E

A portable trolley carrying a point gauge of accuracy 0.01 cm was placed on the two rails fixed along the flume top. At a flat bed section of the channel (e.g. the section 350 cm from the inlet box), the water depth $D'(\text{cm})$ was measured using this point gauge to give the energy head

$$E = D + \frac{q^2}{2gD^2} \text{ cm.} \quad (5.2)$$

C Free Surface

The point gauge mentioned above was used to measure the water depth at every 5 cm horizontal interval along the centre line of the curved bed model.

D Bed Pressure, $p_o/\rho g$

Along the centre line of the curved bed model, 0.32 cm ($1/8 \text{ in}$) dia. copper piezometer tapings were fixed at 5 cm horizontal intervals (c.f. figure 5.2); these were connected by long plastic tubes ($0.63 \text{ cm} = 1/4 \text{ in}$ internal dia.) to vertical water-piezometers ($0.63 \text{ cm} = 1/4 \text{ in}$ external dia. glass tubes) of reading accuracy 0.1 cm .

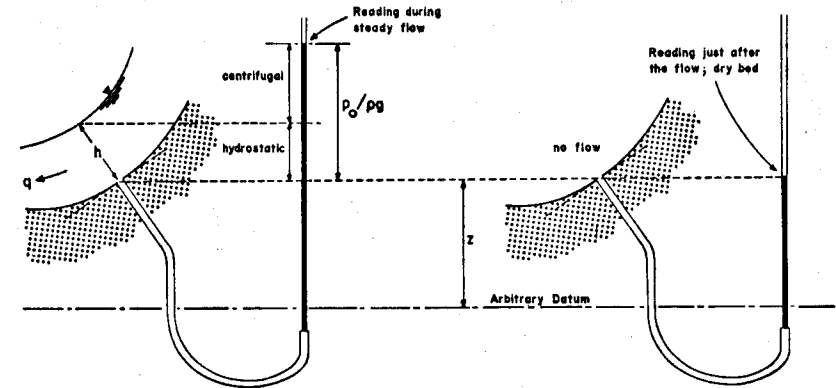
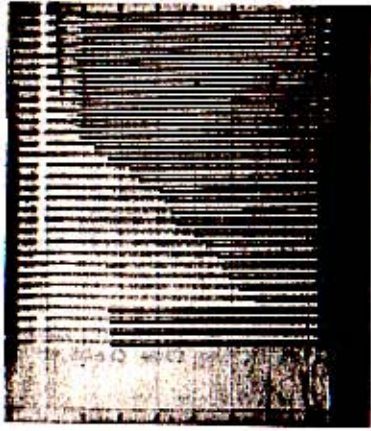


Figure 5.3 Reading the bed pressure

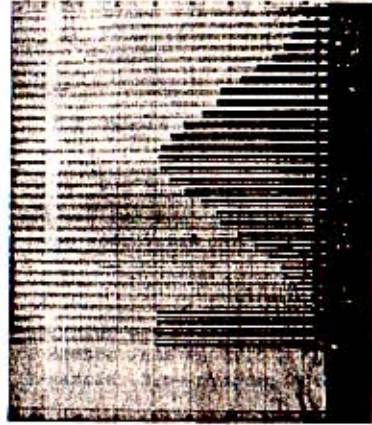
As depicted in figure 5.3, the recorded piezometric level difference between the steady flow and the dry bed condition (i.e. just after slowly draining all water from the flume) gave the bed pressure head $p_o/\rho g$ —c.f. Plate-I.

E Flow Pattern

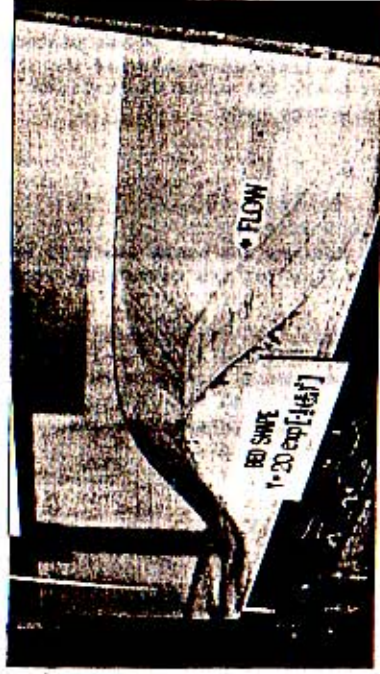
Potassium permanganate solution was injected from an overhead container through a 0.15 cm dia. nozzle at different points in the flow field, to trace the flow pattern—c.f. Plates-II & III.



Piezometric levels
for steady flow: $z + p_0/\rho g$



Piezometric levels
for no flow: z



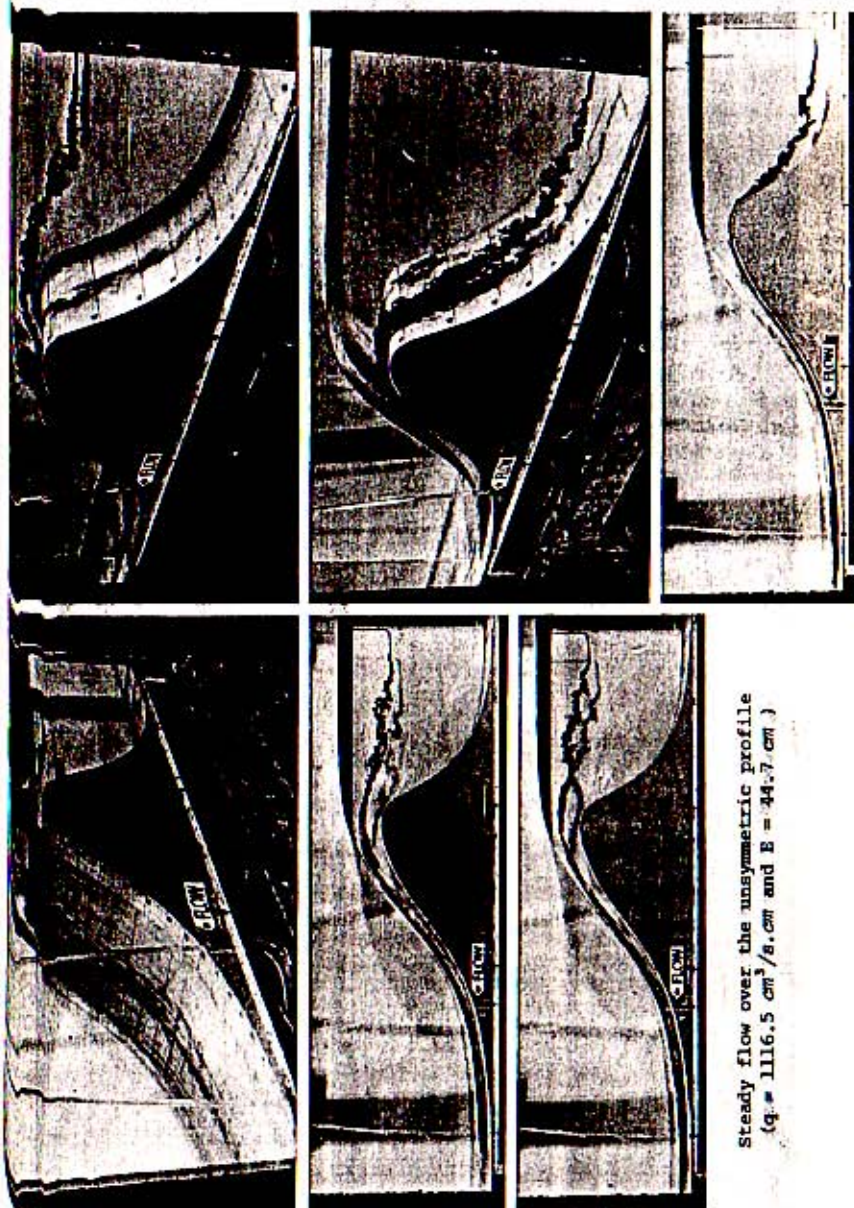
Piezometer tappings upstream



Piezometer tappings downstream



Steady flow over the symmetric profile
($q = 1119.7 \text{ cm}^3/\text{s}\cdot\text{cm}$ and $E = 34.8 \text{ cm}$)



Steady flow over the unsymmetric profile
($q = 1116.5 \text{ cm}^3/\text{s}$, cm and $E = 44.7 \text{ cm}$)

5.3 Experimental Data and Theory

Although the theory defines the free surface by the coordinate n normal to the bed, experimental location of the free surface was made using the vertical coordinate z . Vertical measurements are technically easier to control than measurements normal to the bed which involve varying the inclination of the gauge from point to point, and we compute the depth normal to the bed corresponding to the experimentally recorded vertical depth. As shown in figure 5.4, at point X_1 the vertical depth D_1 on the point gauge gives the experimental free surface coordinates $(X_1, Z_1 \equiv \zeta_1 + D_1)$, and we compute the theoretical free surface location (x_1, z_1) on the same bed-normal through (X_1, Z_1) as follows.

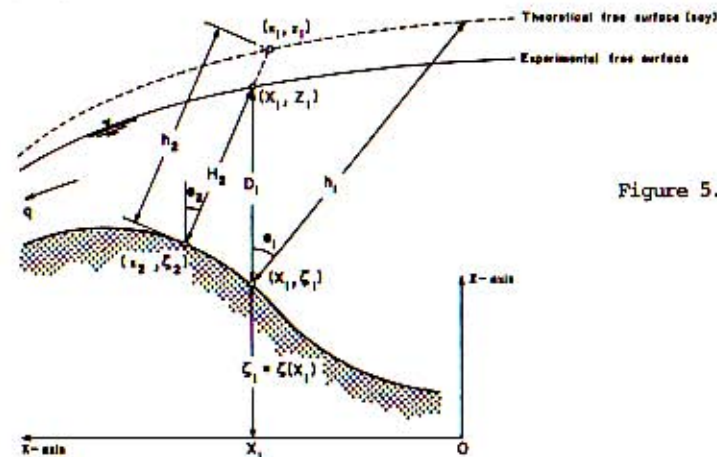


Figure 5.4

Given the bed profile $\zeta(x)$, the solution of

$$\frac{\zeta(x) - Z_1}{x - X_1} \zeta'(x) + 1 = 0 \quad (5.3)$$

is the base $(x_2, \zeta_2 \equiv \zeta(x_2))$ of this bed-normal, and at this point we have

$$\tan \theta_2 = \zeta'(x_2), \quad (5.4)$$

$$\kappa_2 = \zeta''(x_2) \cos^3 \theta_2, \quad (5.5)$$

the experimental flow depth

$$H_2 = \sqrt{(X_1 - x_2)^2 + (Z_1 - \zeta_2)^2}, \quad (5.6)$$

and

$$X_{\text{experi.}} = \kappa_2 H_2. \quad (5.7)$$

³ Upper case denote the experimental values, and lower case the theoretical values.

The theoretical χ is the solution of (4.4); that is

$$\gamma(\chi) = \alpha_2 + \beta_2 \chi, \quad (5.8)$$

where from (4.5), $\alpha_2 \equiv 2g(E-\zeta_2)/(qK_2)^2$ and $\beta_2 \equiv -2g\cos\theta_2/(q^2K_2^3)$. The theoretical flow depth is

$$h_2 = \chi_{\text{theory}} / K_2, \quad (5.9)$$

hence the theoretical location of the free surface is given by

$$\left. \begin{aligned} x_1 &= x_2 - h_2 \sin\theta_2 \\ z_1 &= \zeta_2 + h_2 \cos\theta_2 \end{aligned} \right\} \quad (5.10)$$

As previously described, the bed pressure was measured by a piezometer. Since $u_0 = -qK/\ln(1-\chi)$, from (3.29) the theoretical bed pressure at X_1 is given by

$$\frac{p_0 - p_h}{\rho g} = \frac{\cos\theta}{K} \chi + \frac{q^2 K^2}{2g} \chi(2-\chi)\gamma(\chi), \quad (5.11)$$

\uparrow \uparrow
 Hydrostatic part Centrifugal part

where χ is the solution of

$$\gamma(\chi) = \alpha_1 + \beta_1 \chi, \quad (5.12)$$

in which $\alpha_1 \equiv 2g(E-\zeta_1)/(qK_1)^2$, $\beta_1 \equiv -2g\cos\theta_1/(q^2K_1^3)$; $\tan\theta_1$ and K_1 are respectively the bed slope and curvature at X_1 (c.f. figure 5.4), calculated by similar formulae as (5.4) and (5.5).

Finally, the experimental and theoretical Froude numbers were calculated from (4.7); i.e.

$$F = \sqrt{\frac{2}{\beta_2} \frac{1 + \ln(1-\chi)}{(1-\chi)\ln(1-\chi)^3}} \quad (5.13)$$

[Newton-Raphson iteration was used to solve (5.3), (5.8) and (5.12).]

5.4 Results and Discussion

5.4A Symmetric Profile

Figures 5.5 to 5.9 show the experimental and theoretical free surface and bed pressure for various q and E . (Although not shown, the theoretical bed pressure profiles are also *symmetric* about $x = 0$.) Agreement is excellent, although for larger q the theoretical free surface is slightly below the experimental points in the subcritical region; the inadequacy of the shallow-flow approximation where the flow is deep probably accounts for this. The critical flow occurs exactly at the crest, as predicted by Theorem(2) (see

also figure 5.10). Near the crest in the subcritical region, the experimental points lie below the theoretical free surface of subcritical flow as the flow accelerates into a *transition region* from sub to supercritical flow. For low q , no solution of (4.4) exists near the *transition point*—c.f. the discontinuity at the crest in figures 5.8 and 5.9. Change of velocity gradient may be large in the transition region, so that the basic assumptions of the Dressler equations are questionable (viz. *irrotational inviscid flow*).

TABLE-1

q $\text{cm}^3/\text{s.cm}$	E cm	$\chi_{\min.}$			$\chi_{\max.}$		
		experi.	theory	$x(\text{cm})$	experi.	theory	$x(\text{cm})$
1119.7	34.8	-0.380	-0.385	-5	0.427	0.417	-55
1014.4	34.0	-0.360	-0.370	-5	0.413	0.407	-55
770.3	31.7	-0.304	-0.310	-5	0.381	0.377	-55
561.0	29.6	-0.253	-0.256	-10	0.355	0.352	-50
359.9	27.2	-0.201	-0.201	-10	0.328	0.326	-50

Table-1 summarises extreme χ values and their locations, for the flows (various q and E) for which the symmetric profile was tested; and *all* values fall within the range suggested by Dressler (c.f. (2.13)).

Figures 5.5 to 5.9 also show that the total bed pressure is accurately predicted, at least when centrifugal pressure is small. From (5.11), the theoretical centrifugal pressure is

$$p_c = \frac{\rho q^2}{2h^2} \Lambda(\chi), \quad (5.14)$$

where

$$\Lambda(\chi) \equiv \frac{\chi^3(2-\chi)}{[(1-\chi)\ln(1-\chi)]^2}. \quad (5.15)$$

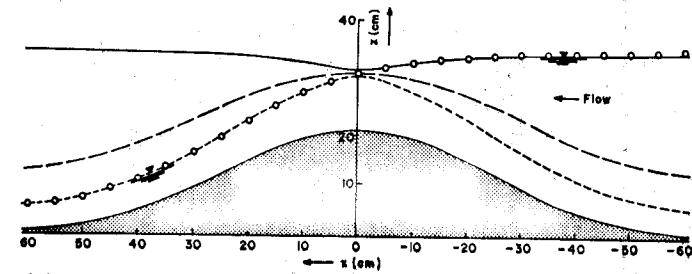
Considering the logarithmic partial differentiation of (5.14) with respect to K , we get

$$\frac{\Delta p_c}{p_c} = \frac{\Lambda'(\chi)}{\Lambda(\chi)} h \Delta K,$$

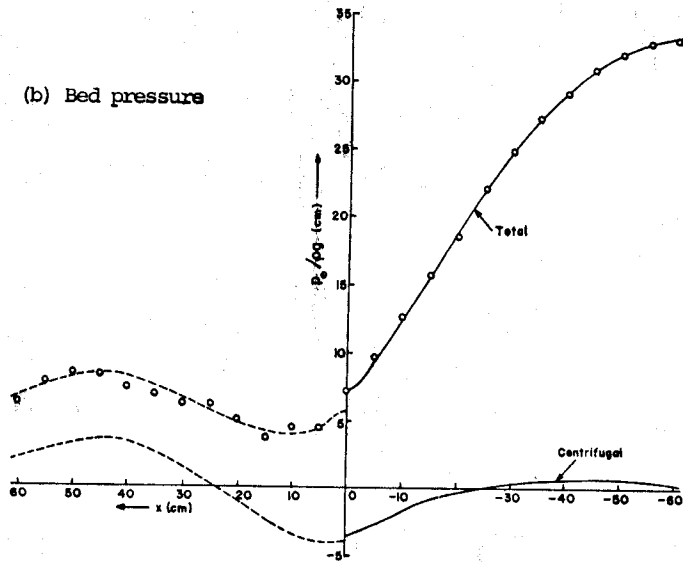
$$\frac{\Delta p_c/p_c}{\Delta K/K} = \frac{\Lambda'(\chi)\chi}{\Lambda(\chi)} = \frac{2[(\chi^2-3\chi+3)\ln(1-\chi)+2\chi-\chi^2]}{(2-\chi)(1-\chi)\ln(1-\chi)}, \quad (5.16)$$

where Δp_c is the error in centrifugal pressure due to an error ΔK in bed curvature.

Figure 5.11 depicts the variation with χ of the ratio between error in the centrifugal pressure and in the bed curvature. Both small local turbulence and curvature error introduced by the flat end piezometer tapings may be the cause of the *systematic error pattern* in the measured bed pressure profiles in the supercritical region—c.f. figures 5.5 to 5.9.



(a) Free surface

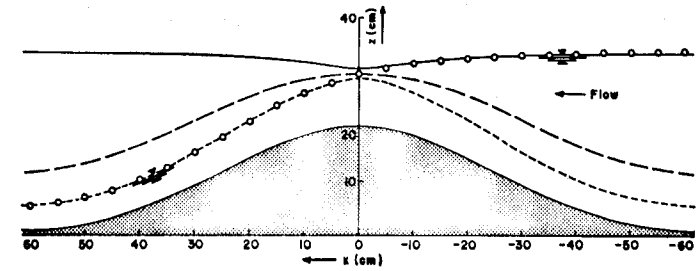


(b) Bed pressure

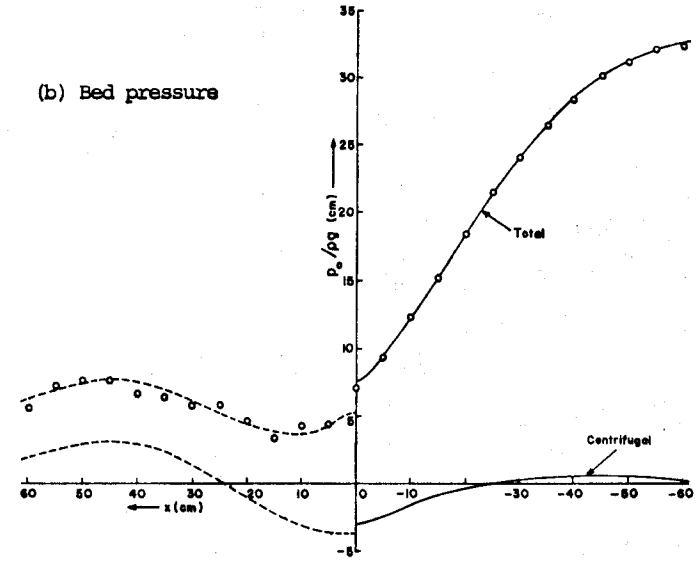
Figure 5.5 Steady flow over the symmetric profile for $q = 1119.7 \text{ cm}^3/\text{s.cm}$ and $E = 34.8 \text{ cm}$

— subcritical
--- critical
- - - supercritical
o experiment

} theory



(a) Free surface

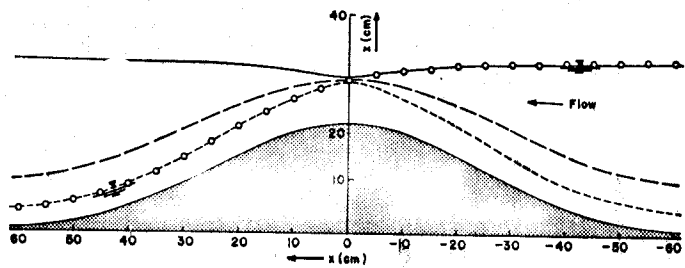


(b) Bed pressure

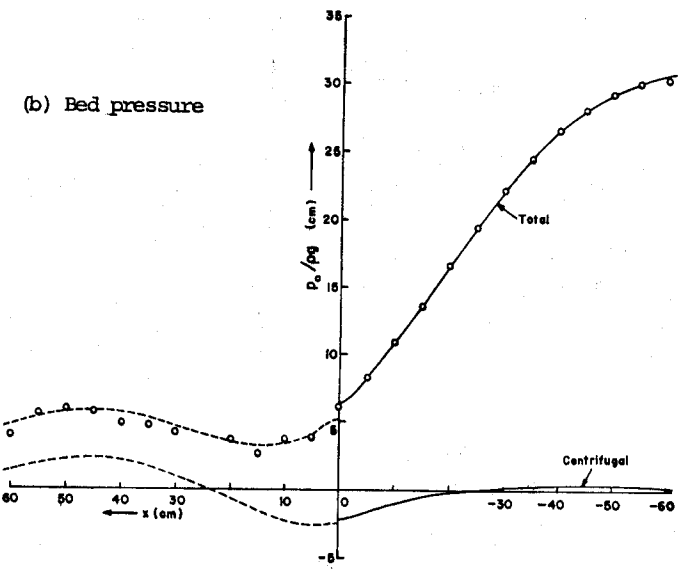
Figure 5.6 Steady flow over the symmetric profile for $q = 1014.4 \text{ cm}^3/\text{s.cm}$ and $E = 34.0 \text{ cm}$

— subcritical
--- critical
- - - supercritical
o experiment

} theory



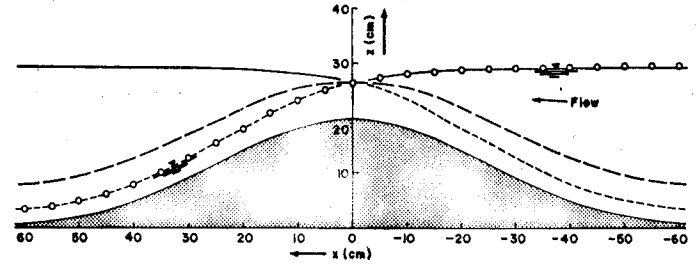
(a) Free surface



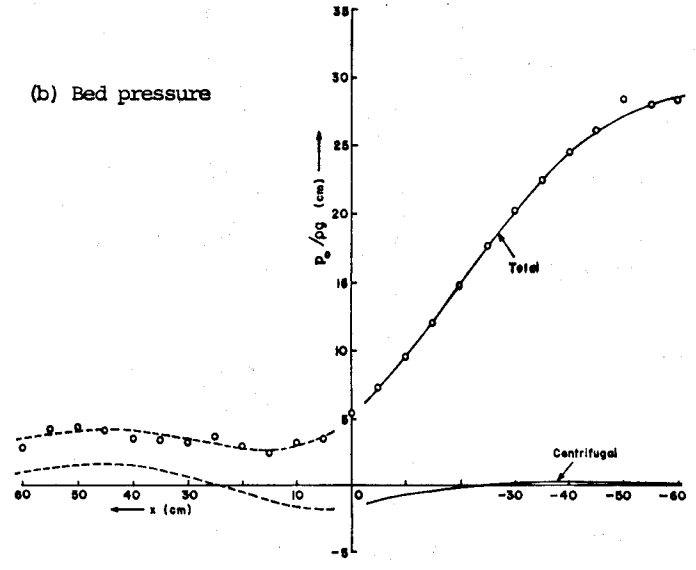
(b) Bed pressure

Figure 5.7 Steady flow over the symmetric profile for $q = 770.3 \text{ cm}^3/\text{s}\cdot\text{cm}$ and $E = 31.7 \text{ cm}$

—	subcritical	} theory
- - -	critical	
· · ·	supercritical	
o	experiment	



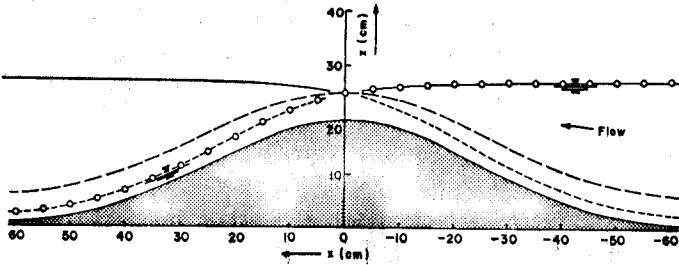
(a) Free surface



(b) Bed pressure

Figure 5.8 Steady flow over the symmetric profile for $q = 561.0 \text{ cm}^3/\text{s}\cdot\text{cm}$ and $E = 29.6 \text{ cm}$

—	subcritical	} theory
- - -	critical	
· · ·	supercritical	
o	experiment	



(a) Free surface

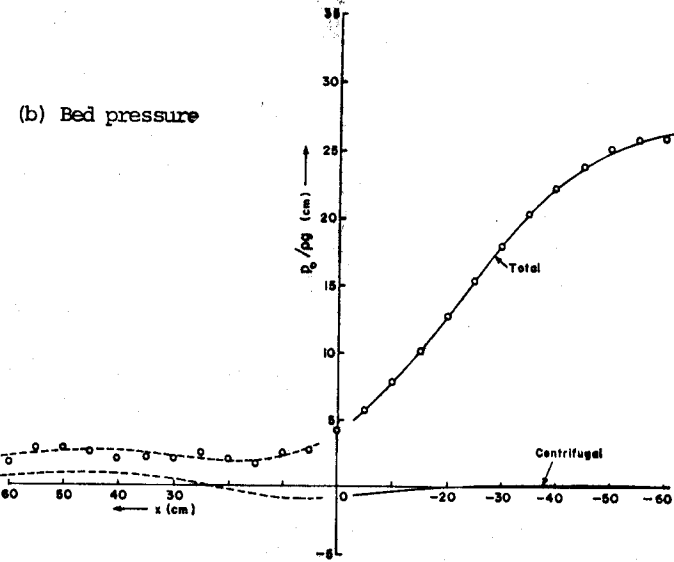


Figure 5.9 Steady flow over the symmetric profile for $q = 359.9 \text{ cm}^3/\text{s.cm}$ and $E = 27.2 \text{ cm}$

— subcritical
- - - critical
- - - supercritical
• experiment

} theory

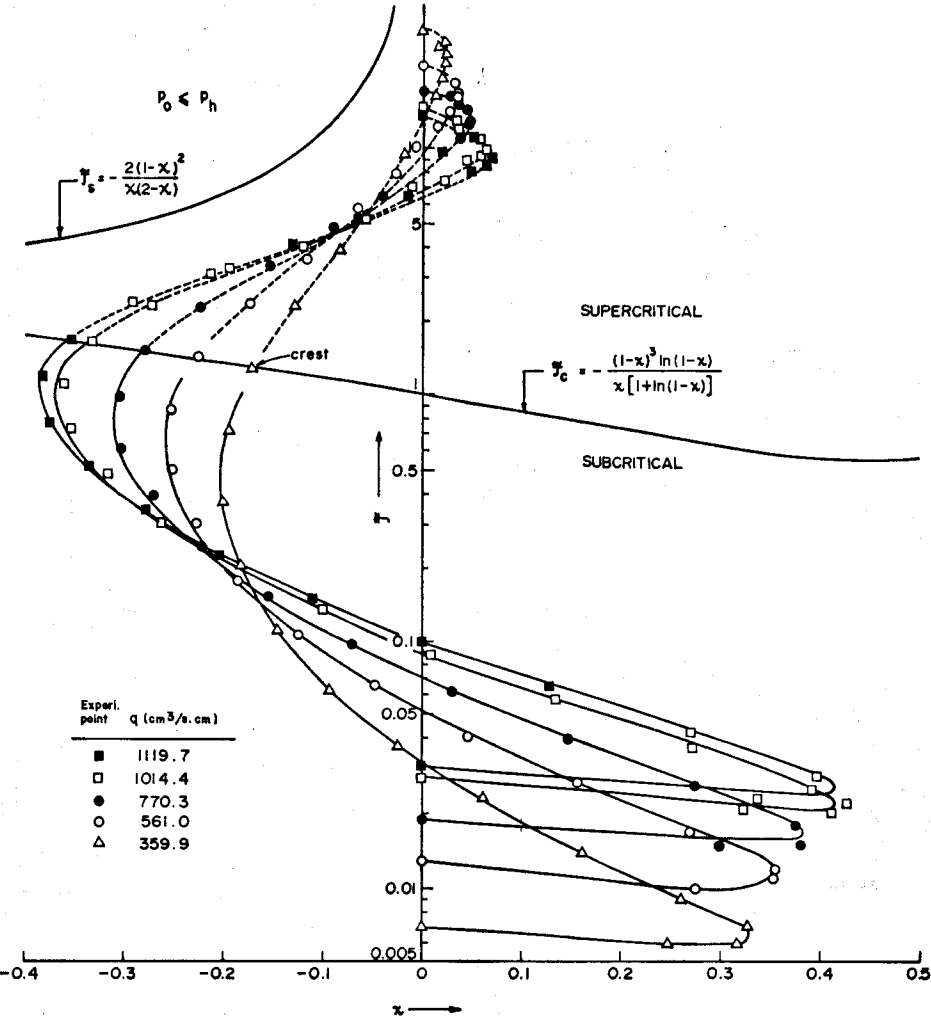


Figure 5.10 Theoretical and experimental f versus x for the symmetric profile

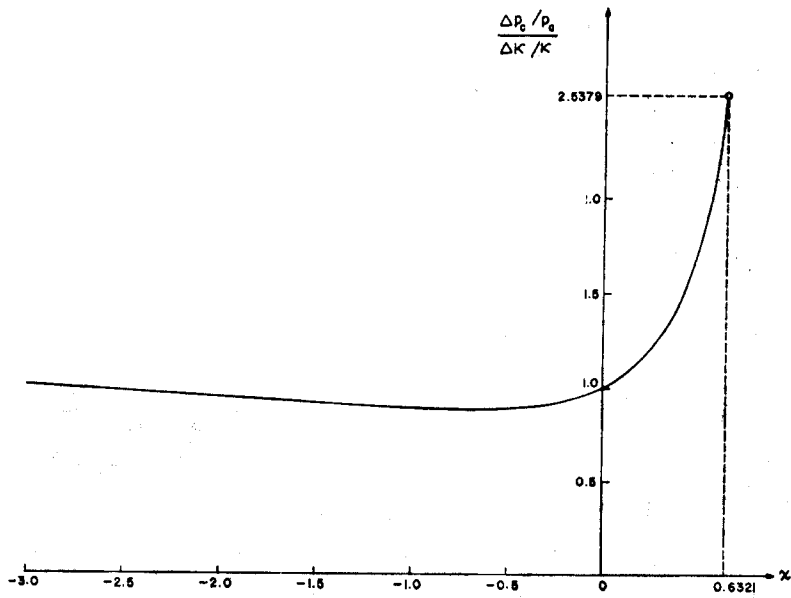


Figure 5.11 Variation of error ratio $\frac{\Delta p_c/p_c}{\Delta K/K}$ versus χ (equation (5.16))

5.4B Unsymmetric Profile

In the symmetric profile, the experimental χ values fell within the range suggested by Dressler (c.f. (2.13)). To test the validity of this range an unsymmetric bed profile, skewed upstream, was designed using a B-splined shape. Figures 5.12 to 5.15 show the experimental and theoretical free surface and bed pressure for different q and E . (Again, the theoretical bed pressure profiles are not continued through the crest.) The transition zone in which the flow changes from sub to supercritical is more extensive in this case, and apparently the critical flow does not occur at the crest but somewhat downstream as expected (c.f. *Theorem*(2), Chapter IV). The following table gives the extreme χ values and their locations. These extremes are outside Dressler's suggested range (2.13), especially for negative χ (c.f. also section 3.7).

TABLE-2

q $cm^3/s.cm$	E cm	$\chi_{min.}$			$\chi_{max.}$		
		experi.	theory	$x(cm)$	experi.	theory	$x(cm)$
1116.5	44.7	-2.808	-3.020	40	0.543	0.543	5
905.3	42.9	-2.236	-2.445	45	0.526	0.527	5
745.8	41.6	-2.070	-2.260	45	0.521	0.523	5
375.0	37.8	-1.608	-1.692	40	0.502	0.506	5

Bed pressure cannot be predicted for certain x (e.g. $3 < x < 8$ cm and $23 < x < 46$ cm for $q = 1116.5$ $cm^3/s.cm$ c.f. figure 5.12), because the χ values are outside the theoretical limit—i.e. $\chi = 0.6321$. The shaded areas in figures 5.12 to 5.15 indicate the domains where no theoretical solution exists. For larger q , the free surface prediction is not unique for certain x near the origin. For instance, when $q = 1116.5$ $cm^3/s.cm$ (c.f. figure 5.12) the bed normals for $8 < x < 23$ cm give the free surface marked by A and for $x > 46$ cm give B. Let us call this phenomenon "normal-crossing"—since it corresponds to bed normals crossing each other. If normal-crossing occurs within the flow, then the bed normals between the respective crossing normals appear redundant for free surface prediction but necessary for bed pressure. If the domain of no solution ($\chi \geq 0.6321$) does not exist within normal-crossing, then these bed normals give a third free surface prediction! Dressler's non-zero Jacobian at the free surface, i.e.

$$J_h \left(\frac{x,z}{s,n} \right) = 1 - \chi > 0,$$

seems insufficient for uniqueness of the predicted free surface.

There is no continuous prediction of either free surface or bed pressure across the transition point (c.f. figures 5.12 to 5.15). Apart from curvature error introduced by the piezometer tappings, other model fabrication curvature errors probably accounts for larger systematic errors in the bed

pressure. (Matched B-splines give a *class-2* curve—i.e. *continuous together with its first two derivatives*—therefore κ is continuous but not $d\kappa/dx$ everywhere; the discontinuity in $d\kappa/dx$ causes the kinks in the *theoretical* bed pressure.)

The theoretical $\chi \equiv \kappa h$ values are plotted against the experimental χ values in figures 5.16 and 5.17, for the symmetric and the unsymmetric profiles respectively. There is remarkable agreement for

$$-2 \leq \kappa h \leq 0.54, \tag{5.17}$$

beyond Dressler's recommended range of validity for his equations.

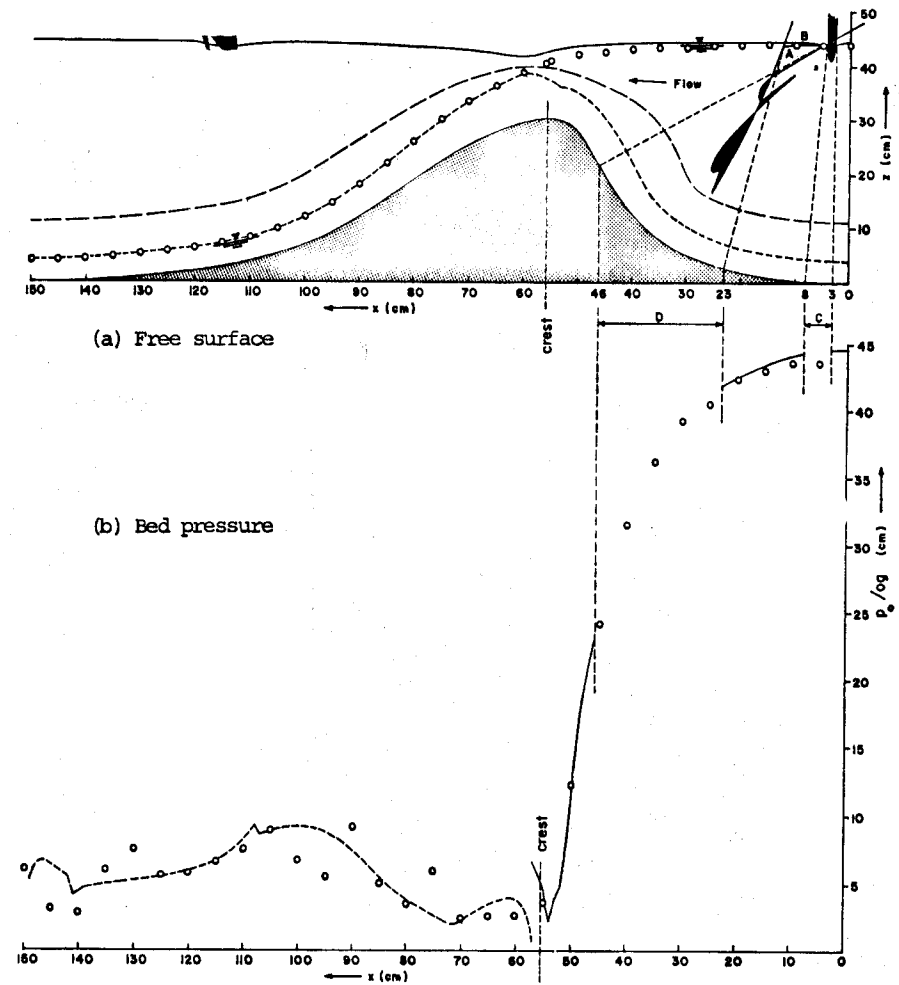


Figure 5.12 Steady flow over the unsymmetric profile for $q = 1116.5 \text{ cm}^3/\text{s.cm}$ and $E = 44.7 \text{ cm}$

- domains where $n \geq 0.6321/\kappa$
- subcritical
- - - critical
- · · supercritical
- } theory
- C, D intervals where bed pressure cannot be predicted
- experiment

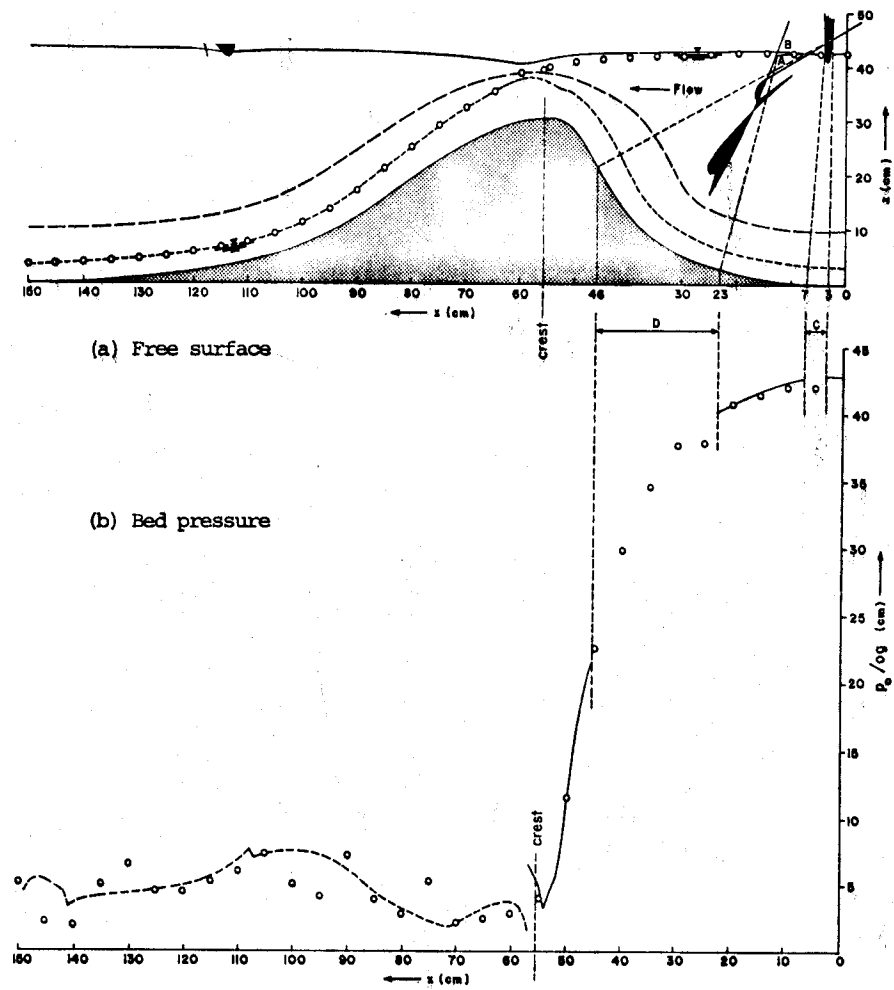


Figure 5.13 Steady flow over the unsymmetric profile for $q = 905.3 \text{ cm}^3/\text{s}\cdot\text{cm}$ and $E = 42.9 \text{ cm}$

■ domains where $n \geq 0.6321/\kappa$
— subcritical
- - - critical
- - - supercritical } theory
C, D intervals where bed pressure cannot be predicted
○ experiment

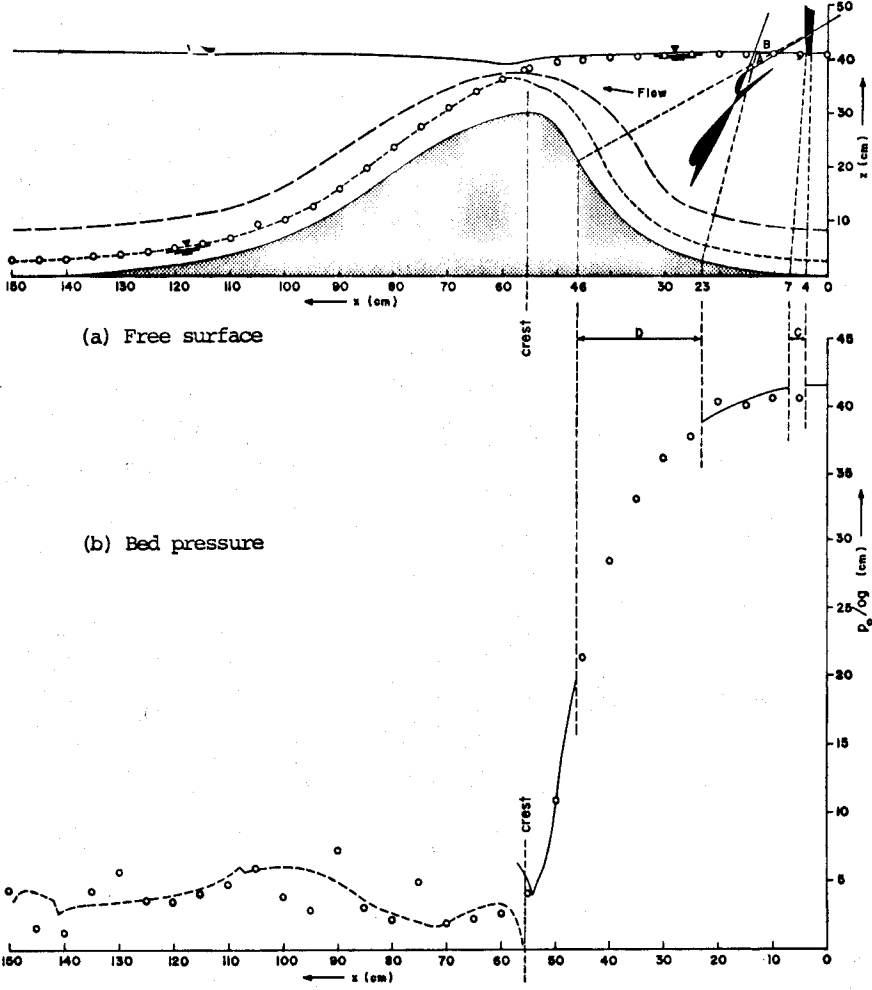


Figure 5.14 Steady flow over the unsymmetric profile for $q = 745.8 \text{ cm}^3/\text{s}\cdot\text{cm}$ and $E = 41.6 \text{ cm}$

■ domains where $n \geq 0.6321/\kappa$
— subcritical
- - - critical
- - - supercritical } theory
C, D intervals where bed pressure cannot be predicted
○ experiment

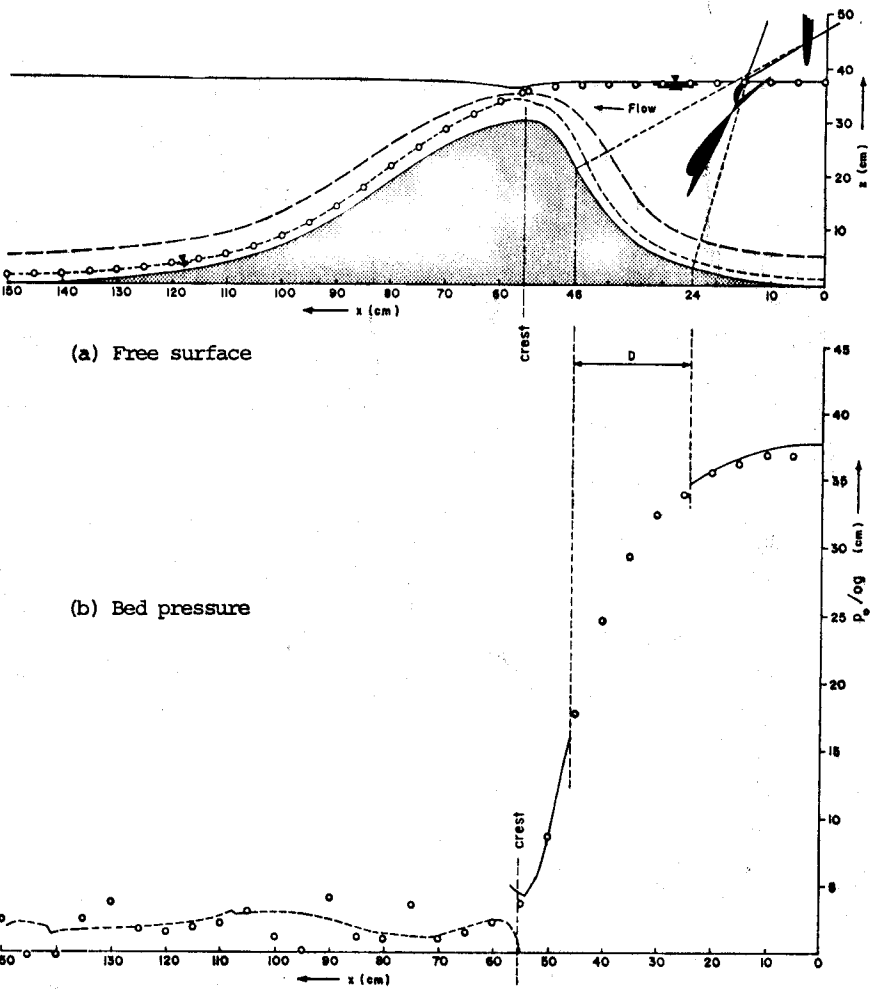


Figure 5.15 Steady flow over the unsymmetric profile for $q = 375.0 \text{ cm}^3/\text{s}\cdot\text{cm}$ and $E = 37.8 \text{ cm}$

- domains where $n \geq 0.6321/k$
- subcritical
- - - critical
- - - - supercritical
- D interval where bed pressure cannot be predicted
- experiment

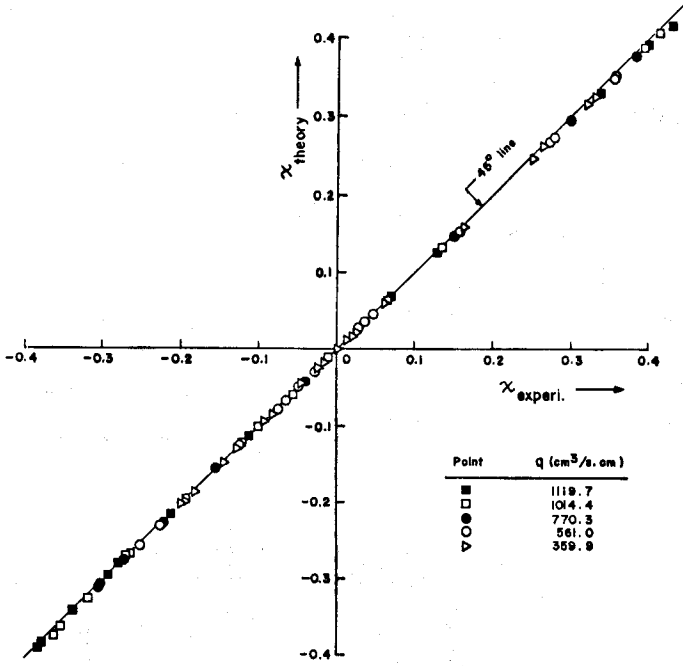


Figure 5.16 Theoretical versus experimental χ for the symmetric profile. The error $(\chi_{\text{experi.}} - \chi_{\text{theory}})$ has mean 0.0013 and standard deviation 0.0023

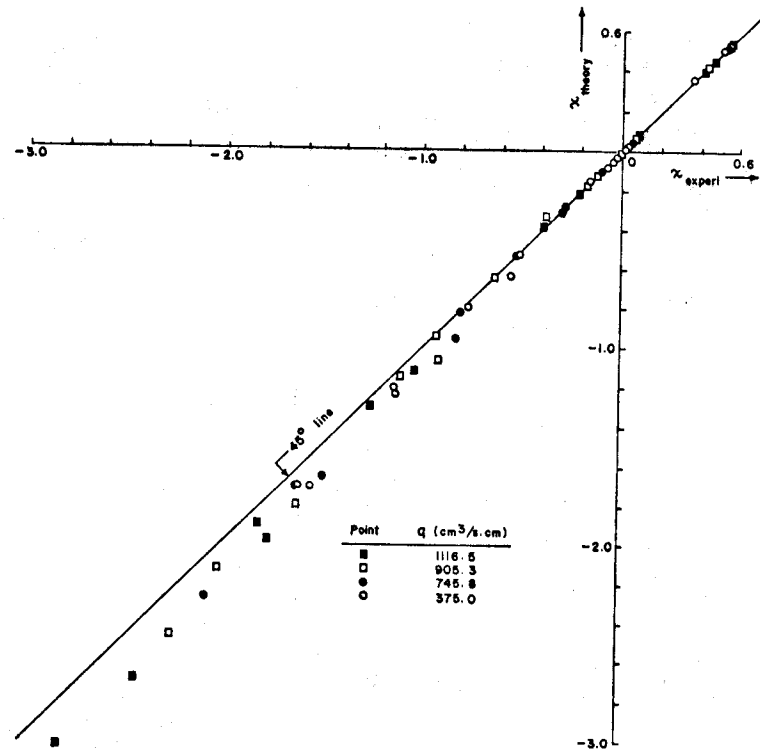


Figure 5.17 Theoretical versus experimental χ for the unsymmetric profile. The error ($\chi_{\text{experi.}} - \chi_{\text{theory}}$) has mean 0.0265 and standard deviation 0.0599

VI CONCLUSIONS AND RECOMMENDATIONS

6.1 Conclusions

From comparison with tested spillway and new experimental data, we reach the following *major conclusions*.

- The Dressler equations are easy to use to accurately predict the free surface and bed pressure (hydrostatic + centrifugal) for steady flow over curved beds, when frictional effects are negligible.
- The equations are valid for convex beds of larger curvature than is the case for concave beds; the experimental range was

$$-2 \leq Kh \leq 0.54$$

with remarkable agreement between the theory and experiment (c.f. Dressler's range: $-0.85 \leq Kh \leq 0.5$).

Other conclusions are:

- the location of the critical flow can be accurately predicted;
- in supercritical flow, any error in the bed curvature affects the bed pressure considerably;
- near the singular point (i.e. transition point), the basic assumptions of the Dressler equations are questionable.

6.2 Recommendations

- The present study emphasises *steady flow*, and solution of the Dressler equations for unsteady flow is recommended for future research. Dynamic pressure variation on spillway crests during the spill of a short duration flood wave, difficult to assess experimentally, is an important engineering problem for example.
- Experimental formulae are available for the "friction factor" $f=f(R, \epsilon)$ of a flat bed, where R and ϵ denote the Reynolds number and relative roughness of the channel surface respectively. Dimensional analysis suggests that for curved beds $f=f(R, \epsilon, Kh)$, and its evaluation is important in order to generalize the existing *Moody diagram* to extend the *Chézy formula* to curved beds. The discussion on roll waves given in *Appendix-B* could then be extended.

APPENDIX-A On the Geometry of Curved Bed Profiles

A.1 Symmetric Profile

The symmetric profile of length 120 cm is described by the normal distribution:

$$\zeta = 20 \exp \left[-\frac{1}{2} \left(\frac{x}{24} \right)^2 \right] \quad (\text{A.1})$$

A.2 Unsymmetric Profile

The unsymmetric profile of length $L = 150$ cm is designed using B-splines (De Boor, 1978) as follows.

Let I_i be x -intervals: $X_i < x \leq X_{i+1}$, and $V_i \equiv (X_i, Y_i)$ be vertices, where $i = 0, 1, \dots, m-1$; $V_0 \equiv (0, 0)$ and $V_m \equiv (L, 0)$. In terms of parameter $s \in [0, 1]$ in I_i , a point $(\xi(s), \zeta(s))$ on the spline curve is given by

$$\eta(s) = \frac{1}{6}(s^3 \ s^2 \ s \ 1) \begin{bmatrix} -1 & 3 & -3 & 1 \\ 3 & -6 & 3 & 0 \\ -3 & 0 & 3 & 0 \\ 1 & 4 & 1 & 0 \end{bmatrix} \begin{bmatrix} V_{i-1} \\ V_i \\ V_{i+1} \\ V_{i+2} \end{bmatrix} \quad (\text{A.2})$$

where $\eta = \xi$ when $V = X$, and $\eta = \zeta$ when $V = Y$. Artificial vertices

$$\left. \begin{aligned} V_{-1} &\equiv 2V_0 - V_1 \\ V_{m+1} &\equiv 2V_m - V_{m-1} \end{aligned} \right\} \quad (\text{A.3})$$

are defined so that the curve has zero curvature at the end points V_0 and V_m . The entire curve from V_0 to V_m is of class-2—i.e. the curve is continuous together with its first two derivatives (so that slope θ and curvature κ , but not necessarily its derivatives, are continuous).

At a given abscissa x , to find the slope $\tan \theta \equiv d\zeta/d\xi$ and the curvature $\kappa \equiv (d^2\zeta/d\xi^2) \cos^3 \theta$, we solve

$$\xi(s) - x = 0 \quad (\text{A.4})$$

for s (using Newton-Raphson iteration) to find ξ', ζ', ξ'' and ζ'' (where prime denotes differentiation with respect to s) so that

$$\left. \begin{aligned} \frac{d\zeta}{d\xi} &= \zeta' / \xi' \\ \frac{d^2\zeta}{d\xi^2} &= \zeta'' / (\xi')^2 - [\xi'' / (\xi')^2] \frac{d\zeta}{d\xi} \end{aligned} \right\} \quad (\text{A.5})$$

For the unsymmetric profile we take $m = 11$ and:

i	X_i	Y_i
0	0.	0.
1	9.225681	-0.109890
2	31.011056	3.846153
3	40.140415	12.318963
4	45.675620	20.524091
5	48.524623	26.700479
6	53.408628	32.155536
7	71.438746	26.294730
8	88.980463	11.732882
9	107.890720	2.787639
10	141.578144	0.008453
11	150.	0.

APPENDIX-B Roll Waves

B.1 Roll Waves in Flat Bed Open Channels

It has been observed that in steep channels steady, gradually varied, turbulent flow theory fails beyond a certain critical Froude number as free surface instability results in *roll waves* of various wave-length, amplitude and phase-velocity (Cornish 1934; Rouse 1938). Dressler (1949) showed theoretically that roll waves cannot occur if the flow resistance is too large, although they cannot be formed without it. He considered Saint-Venant equations (c.f. p.2-1) with resistance given by the Chézy formula for wide channels (c.f. p.2-4), and obtained a simple necessary condition for the initiation of roll waves viz. $4g/C^2 < \tan\theta$ (g -gravity, C -constant Chézy coefficient, and θ -channel inclination), or equivalently the Froude number $F > 2$.

Iwasa (1954) described one-dimensional flow in a prismoidal channel by continuity and momentum equations (c.f. figure B.1):

$$A_t + (UA)_x = 0, \quad (B.1)$$

$$U_t + \beta U U_x + g \cos\theta H_x + (1-\beta) \frac{U}{A} A_t = g \sin\theta - \frac{\tau}{\rho R}, \quad (B.2)$$

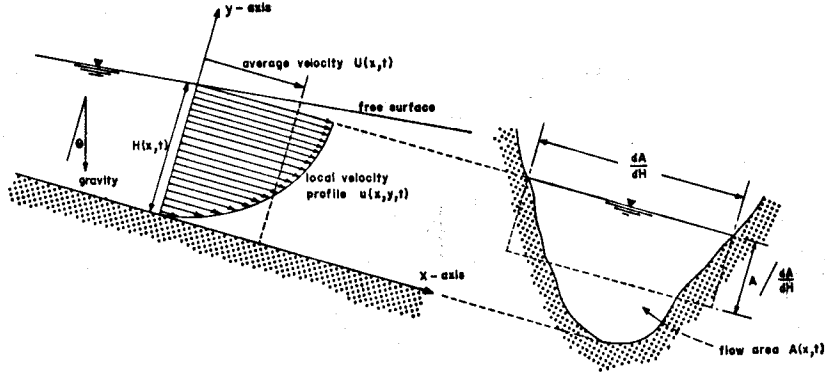


Figure B.1

where

A - flow area	x - coordinate along flat bed
g - gravity	y - coordinate normal to bed
H - flow depth	τ - shear stress at channel surface
R - hydraulic radius	ρ - fluid density
t - time	θ - channel inclination
u - local velocity	$\beta \equiv \frac{1}{U^2 A} \int_A u^2 dA$ - momentum coefficient
U - average velocity	

and partial derivatives with respect to x and t are denoted by suffices.

He established a necessary condition for roll waves:

$$F > \left\{ \left[\frac{A}{2f} \frac{dR}{dA} \left(\frac{\partial f}{\partial R} - \frac{f}{R} \right) - (\beta-1) \right]^2 - \beta(\beta-1) \right\}^{-1/2}, \quad (B.3)$$

where the Froude number and friction factor are given by

$$F \equiv U / \sqrt{g \left(A \frac{dA}{dH} \right) \cos\theta}; \quad f \equiv 8\tau/\rho U^2. \quad (B.4)$$

Since f is assumed to vary (i.e. Chézy coefficient not constant, unlike Dressler's derivation), (B.3) gives a family of curves relating the critical Froude number, Reynolds number and the friction factor (c.f. Rouse (1965)).

Berlamont (1976) studied the roll wave phenomenon taking into account vertical velocity and acceleration. Assuming that

- the velocity profiles are "similar" in all cross-sections;¹
- the flow is gradually varied;
- the bed shear stress $\tau = f(U,H)U^2/8$;
- the product of lower order derivatives of U and H are small compared with the higher order derivatives;

he integrated the continuity and momentum equations to yield:

$$H_t + (UH)_x = 0, \quad (B.5)$$

$$U_t + \beta U U_x + g \cos\theta H_x + (1-\beta) \frac{U}{H} H_t + \frac{HU^2}{3} \left(\frac{a}{U} H_{xxt} + \frac{b}{U} H_{xxt} + c H_{xxt} \right) = g \sin\theta - f \frac{U^2}{8H}, \quad (B.6)$$

where constants a , b and c depend upon the shape assumed for the velocity profiles, and the Darcy-Weisbach friction factor f is calculated from the White-Colebrook (Thijssse) formula:

$$\frac{1}{\sqrt{f}} = -2.03 \log_{10} \left(\frac{k_s/R}{12.20} + \frac{3.03}{R\sqrt{f}} \right) \quad (B.7)$$

Here the Reynolds number $R \equiv 4UH/\nu$ (ν -kinematic viscosity), and k_s is characteristic bed roughness height.

Berlamont (1976) derived a fourth-order linearised equation for small amplitude disturbances of uniform flow. He observed a *lower critical Froude number* F_c for roll wave formation as a function of R , k_s/R , velocity distribu-

¹ i.e. $u(x,y,t) = \phi\left(\frac{y}{H}\right) U(x,t)$. This is exact for laminar flow (parabolic velocity profile) and holds approximately for turbulent flow.

tion and wave-length λ (c.f. figure B.2); and also explained the existence of an upper critical Froude number, beyond which no roll waves are formed.

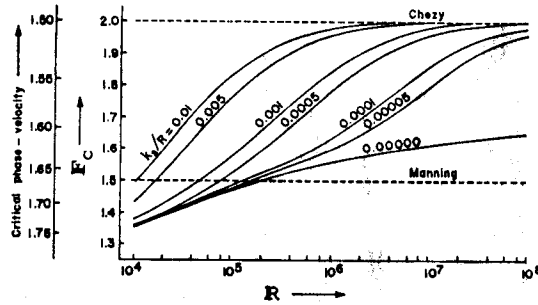


Figure B.2 Lower critical Froude number for $\beta=1$, $\lambda=\infty$ (after Berlamont, 1976)

B.2 Roll Waves in Curved Bed Open Channels

B.2A General Equation for Lower Critical Froude Number

Shallow-flow in a curved bed open channel is defined by the Dressler equations (c.f. p.3-9)

$$\Omega \frac{\partial h}{\partial t} + \frac{\partial q}{\partial s} = 0, \quad (B.8)$$

$$\frac{\partial u_o}{\partial t} + g \frac{\partial E}{\partial s} = F, \quad (B.9)$$

where

$$\left. \begin{aligned} \Omega &\equiv 1 - kh \\ u_o(q, h, s) &\equiv -qK / \ln \Omega \\ E(q, h, s) &\equiv \zeta + h \cos \theta + \frac{q^2 K^2}{2g} (\Omega \ln \Omega)^{-2} \end{aligned} \right\} \quad (B.10)$$

and $F(q, h, s)$ denotes frictional dissipation at the rough channel surface. In this Section, the stability of steady flow is considered.

If $\bar{q} = \text{constant}$ and $\bar{h}(s)$ denote the steady flow, the perturbed quantities are

$$q(s, t) = \bar{q} (1 + \phi) \quad (B.11)$$

$$h(s, t) = \bar{h} (1 + \eta)$$

where $\phi(s, t)$, $\eta(s, t)$ are small (i.e. $|\phi|, |\eta| \ll 1$). Introducing (B.11) into (B.8) and (B.9), and retaining only linear terms in ϕ , η we get

$$\eta_t = -\frac{\bar{q}}{\Omega \bar{h}} \phi_s, \quad (B.12)$$

$$\left[\left(\frac{\partial u_o}{\partial q} \right) \phi + \left(\frac{\partial u_o}{\partial h} \right) \eta \right]_t + g \left[\left(\frac{\partial E}{\partial q} \right) \phi + \left(\frac{\partial E}{\partial h} \right) \eta \right]_s = \left(\frac{\partial F}{\partial q} \right) \phi + \left(\frac{\partial F}{\partial h} \right) \eta \quad (B.13)$$

From (B.10)

$$\left(\frac{\partial u_o}{\partial q} \right) \phi = \bar{u}_o \quad \left(\frac{\partial u_o}{\partial h} \right) \eta = -\frac{\bar{\Omega} \bar{h}}{\bar{q}} \bar{u}_h^2 \quad (B.14)$$

$$\left(\frac{\partial E}{\partial q} \right) \phi = \bar{u}_h^2 \quad \left(\frac{\partial E}{\partial h} \right) \eta = g \bar{h} (1 - F^2) \cos \theta$$

where $\bar{\Omega} \equiv 1 - k\bar{h}$, $\bar{u}_h = \bar{u}_o / \bar{\Omega}$, and F is given by (3.35). Partial derivatives with respect to s and t are denoted by subscripts.

Differentiating (B.13) with respect to t and eliminating η_t using (B.12), we get a second order linear equation in ϕ :

$$\bar{u}_o \phi_{tt} + 2\bar{u}_h^2 \phi_{ts} + L \phi_{ss} + M \phi_t + N \phi_s = 0, \quad (B.15)$$

where

$$\left. \begin{aligned} L &\equiv -\frac{\bar{q}}{\bar{\Omega}} (1 - F^2) g \cos \theta \\ M &\equiv (\bar{u}_h^2)_s - \left(\bar{q} \frac{\partial F}{\partial q} \right) \\ N &\equiv L_s + \frac{\bar{q}}{\bar{\Omega} \bar{h}} \left(\bar{h} \frac{\partial F}{\partial h} \right) \end{aligned} \right\} \quad (B.16)$$

Equation (B.15) is general, and from its solution one may determine the lower critical Froude number based on a stability criterion.

B.2B Special Case: "Plane Wave" Approximation

Let us suppose that \bar{h}_s is small, to consider a "plane wave" approximation

$$\phi(s, t) = a \exp[i\alpha(s - \sigma t)] \quad (B.17)$$

in which $\sigma = \sigma_r + i\sigma_i$ is a complex constant; $\alpha, \sigma_r, \sigma_i$ and σ_i are real constants and $i = \sqrt{-1}$. (B.16) now simplifies to ($\bar{h}_s = 0$, $\bar{K}_s = 0$)

$$\left. \begin{aligned} L &\equiv -\frac{\bar{q}}{\bar{\Omega}} (1 - F^2) g \cos \theta \\ M &\equiv -\left(\bar{q} \frac{\partial F}{\partial q} \right) \\ N &\equiv \frac{\bar{q}}{\bar{\Omega}} g K s \sin \theta + \frac{\bar{q}}{\bar{\Omega} \bar{h}} \left(\bar{h} \frac{\partial F}{\partial h} \right) \end{aligned} \right\} \quad (B.18)$$

since $d\theta/ds = \kappa$, and $\bar{q}\bar{n}^{-1}F^2 \cos\theta$ is a function of $\kappa\bar{h}$ only.

Setting (B.17) in (B.15), taking real and imaginary parts we get ($\alpha \neq 0$)

$$u_0 \alpha (\sigma_i^2 - \sigma_r^2) + 2u_h^2 \alpha \sigma_r + M \sigma_i - L \alpha = 0, \quad (B.19)$$

$$2u_0 \alpha \sigma_r \sigma_i - 2u_h^2 \alpha \sigma_i + M \sigma_r - N = 0, \quad (B.20)$$

on omitting the bars for the steady flow quantities.

The stability depends on the sign of σ_i ; if $\sigma_i > 0$, the amplitude will grow with time and the flow will be *unstable*. Considering *marginal stability* ($\sigma_i = 0$), from (B.19) and (B.20) we get

$$u_0 \sigma_r^2 - 2u_h^2 \sigma_r + L = 0, \quad (B.21)$$

$$\sigma_{r,c} = N/M, \quad (B.22)$$

where $\sigma_{r,c}$ denotes the *critical phase-velocity*; eliminating $\sigma_{r,c}$ we have

$$u_0 N^2 - 2u_h^2 N M + L M^2 = 0, \quad (B.23)$$

to be solved for the *critical Froude number* F_c below which no roll waves are formed.

Setting (B.18) in (B.23), and using $u_0^2/(gh \cos\theta) = \tilde{f} = \tilde{f}_c F^2$, $q/u_0 = -\kappa^{-1} \ln \Omega$, and $\Omega = 1-\chi$ (c.f. Section 3.6) we get

$$F_c = \sqrt{\frac{1 + \ln(1-\chi)}{\ln(1-\chi) + \left[1 - D \frac{(1-\chi) \ln(1-\chi)}{\chi}\right]^2}} \quad (B.24)$$

where

$$D \equiv \frac{g\chi \sin\theta + h\partial F/\partial h}{q\partial F/\partial q} \quad (B.25)$$

For the flat bed limit ($\kappa \rightarrow 0$), (B.24) reduces to

$$F_c = 1/|1+D|. \quad (B.26)$$

If $F \equiv \lambda u^2/h^m = \lambda q^2/h^{m+2}$, then $\partial F/\partial h = -(m+2)F/h$, $\partial F/\partial q = 2F/q$; and hence (B.26) gives

$$F_c = 2/m \quad (B.27)$$

This recovers the familiar results $F_c = 2$ and 1.5, respectively, for *Chézy* ($m=1$) and *Manning* ($m=4/3$) resistance terms (c.f. figure B.2).

REFERENCES

- ACKERS, P., WHITE, W.P., PERKINS, J.A. and HARRISON, A.J.M. (1978), *Weirs and Flumes for Flow Measurement*, John Wiley & Sons Ltd., Chichester.
- ALI, K.H.M. (1972), *Flow Over Rounded Spillways*, Proc. ASCE, Vol. 98, No. HY2, pp. 365-380.
- BALLOFFET, A. (1961), *Pressures on Spillway Flip Buckets*, Proc. ASCE, Vol. 87, No. HY5, pp. 87-98.
- BERLAMONT, J. (1976), *Roll Waves in Inclined Rectangular Open Channels*, Proc. International Symposium on Unsteady Flow in Open Channels, Newcastle-Upon-Tyne, England, pp. A2-13.
- CASSIDY, M. (1965), *Irrotational Flow Over Spillways of Finite Height*, Proc. ASCE, Vol. 91, No. EM6, pp. 155-173.
- CHOW, V.T. (1959), *Open Channel Hydraulics*, McGraw-Hill Book Company Inc., N.Y., pp. 370-380.
- CORNISH, V. (1934), *Ocean Waves and Kindred Geophysical Phenomena*, Cambridge University Press, London.
- DE BOOR, C. (1978), *A Practical Guide to Splines*, Springer-Verlag, N.Y.
- DOBSON, R.S. (1967), *Some Applications of Digital Computer to Hydraulic Engineering Problems*, Dept. of Civil Eng., Stanford University, California, Tech. Report No. 80, pp. 36-39.
- DOUMA, J.H. (1954), *Discussion on Design of Side Walls in Chutes and Spillways*, Trans. ASCE, Vol. 119, pp. 364-368.
- DRESSLER, R.F. (1949), *Mathematical Solution of the Problem of Roll Waves in Inclined Open Channels*, Comm. Pure & Appl. Math., Courant Institute, N.Y., Vol. II, No. 2, pp. 149-194.
- DRESSLER, R.F. and POHLE, F.V. (1953), *Resistance Effects on Hydraulic Instability*, Comm. Pure & Appl. Math., Courant Institute, Vol. VI, No. 1, pp. 93-96.
- DRESSLER, R.F. (1958), *Unsteady Nonlinear Waves in Sloping Channels*, Mathematical Physics Section, Nat. Bur. Stand., pp. 186-198.
- DRESSLER, R.F. (1978), *New Nonlinear Shallow-Flow Equations with Curvature*, J. Hydraulic Research, Vol. 16, No. 3, pp. 205-220.
- ESCOFFIER, F.F. (1958), *Transition Profiles in Nonuniform Channels*, Trans. ASCE, Vol. 123, pp. 43-65.
- FOX, J.A. (1977), *Hydraulic Analysis of Unsteady Flow in Pipe Networks*, M, op. 177-200.

- FRIEDRICHS, K.O. (1948), *On the Derivation of the Shallow Water Theory*, Comm. Pure & Appl. Math., Courant Institute, N.Y., Vol. I, No. 1, pp. 81-87.
- FRIEDRICHS, K.O. and DRESSLER, R.F. (1961), *A Boundary-Layer Theory for Elastic Plates*, Comm. Pure & Appl. Math., Courant Institute, N.Y., Vol. XIV, No. 1.
- HENDERSON, F.M. and TIERNEY, D.C. (1963), *Flow at the Toe of a Spillway*, La Houille Blanche, No. 1, pp. 42-50.
- HENDERSON, F.M. (1966), *Open Channel Flow*, Macmillan Publishing Co., Inc., N.Y., pp. 180-191.
- IWASA, Y. (1954), *The Criterion for Instability of Steady Uniform Flows in Open Channels*, Memoirs, Faculty of Eng., Kyoto University, Vol. 16, No. VI.
- JEFFREYS, H. (1925), *The Flow of Water in an Inclined Channel of Rectangular Section*, Phil. Mag., London, S. 6, Vol. 49, No. 293, pp. 793-807.
- KELLER, J.B. (1948), *The Solitary Wave and Periodic Waves in Shallow Water*, Comm. Pure & Appl. Math., Courant Institute, N.Y., Vol. I, No. 4, pp. 323-339.
- KYRALA, A. (1967), *Theoretical Physics: Applications of Vectors, Matrices, Tensors and Quaternions*, W.B. Saunders Company, Philadelphia, pp. 135-165.
- LAMB, H. (1945), *Hydrodynamics*, Dover, N.Y.
- MOAYERI, M.S. (1973), *Flow in Open Channels with Smooth Curved Boundaries*, Proc. ASCE, Vol. 99, No. HY12, pp. 2217-2232.
- PLAAT, O. (1971), *Ordinary Differential Equations*, Holden-Day, Inc., San Francisco, pp. 182-257.
- PRANDTL, L. (1905), *Verhandlungen des dritten internationalen Mathematiker-Kongresses*, Leipzig.
- ROUSE, H. and REID, L. (1935), *Model Research on Spillway Crests, a Study of Pressure Distribution and Discharge as a Function of Crest Design*, Civil Engineering, Vol. 5, No. 1, pp. 10-14.
- ROUSE, H. (1938), *Fluid Mechanics for Hydraulic Engineers*, McGraw-Hill, N.Y.
- ROUSE, H. (1965), *Critical Analysis of Open Channel Resistance*, Proc. ASCE, Vol. 91, No. HY4, pp. 1-25.
- SAINT-VENANT, B. De. (1871), *Comptes Rendus Académie des Sciences, Paris*, Tome 73. July.

- STOKER, J.J. (1948), *Formation of Breakers and Bores*, Comm. Pure & Appl. Math., Courant Institute, N.Y., Vol. I, No. 1.
- WATTERS, G.Z. and STREET, R.L. (1964), *Two-Dimensional Flow Over Sills in Open Channels*, Proc. ASCE, Vol. 90, No. HY4, pp. 107-140.
- WEHAUSEN, J.V. and LAITONE, E.V. (1960), *Surface Waves*, Encyclopedia of Physics, Springer-Verlag, Berlin, Vol. IX, p. 466.

GENERAL REFERENCES

- BATCHELOR, G.K. (1970), *An Introduction to Fluid Dynamics*, University Press, Cambridge.
- BIRKHOFF, G. (1955), *Hydrodynamics, a Study in Logic, Fact, and Similitude*, Dover, N.Y.
- GOLDSTEIN, S. (1965), *Modern Developments in Fluid Dynamics*, Vol. I, Dover, N.Y.
- HOSKING, R.J., JOYCE, D.C. and TURNER, J.C. (1979), *First Steps in Numerical Analysis*, Hodder and Stoughton, London.
- KENNEDY, J.F. and MACAGNO, E.O. (1971), *Selected Writings of Hunter Rouse*, Dover, N.Y.
- LIGHTHILL, M.J. (1978), *Waves in Fluids*, University Press, Cambridge.
- LIN, C.C. (1955), *The Theory of Hydrodynamic Instability*, University Press, Cambridge.
- MCCONNELL, A.J. (1957), *Applications of Tensor Analysis*, Dover, N.Y.
- SERRIN, J. (1959), *Mathematical Principles of Classical Fluid Mechanics*, Encyclopedia of Physics, Springer-Verlag, Berlin, Vol. VII/1, pp. 125-263.
- WHITHAM, G.M. (1974), *Linear and Nonlinear Waves*, John Wiley & Sons, N.Y.

